

Contents lists available at [ScienceDirect](https://www.sciencedirect.com)

Remote Sensing of Environment

journal homepage: www.elsevier.com/locate/rse

Combined use of R-VSPI and VSPI for enhanced quantification of fire severity in south-eastern Australian forests

Aakash Chhabra^{a,b,*}, Christoph Rüdiger^{a,c}, James Hilton^d, Rachael H. Nolan^{e,f}, Eli R. Bendall^e, Marta Yebra^{g,h}, Thomas Jagdhuber^{i,j}

^a Department of Civil Engineering, Monash University, Clayton, VIC 3800, Australia

^b Currently at: NASA Ames Research Center, Moffett Field, CA 94035, USA

^c Bureau of Meteorology, Docklands, VIC 3008, Australia

^d Covey Associates, Maroochydore, Queensland 4558, Australia

^e Hawkesbury Institute for the Environment, Western Sydney University, Locked Bag 1797, Penrith, New South Wales 2751, Australia

^f NSW Bushfire Risk Management Research Hub, Wollongong, NSW 2522, Australia

^g Fenner School of Environment & Society, College of Science, The Australian National University, Canberra, ACT 2600, Australia

^h School of Engineering, College of Engineering and Computer Science, The Australian National University, Canberra, ACT 2600, Australia

ⁱ Microwaves and Radar Institute, German Aerospace Center (DLR), 82234 Weßling, Germany

^j Institute of Geography, Faculty of Applied Informatics, Augsburg University, 86159 Augsburg, Germany

ARTICLE INFO

Keywords:

Fire severity
Sentinel-1
Sentinel-2
Supervised classification
Field-validation

ABSTRACT

Wildfires, intensified by climate change, necessitate advanced methods for accurate and near-real-time fire severity mapping to improve emergency response and post-fire recovery strategies. Satellite remote sensing, combined with supervised learning approaches, enhances the accuracy and efficiency of fire severity mapping. This study introduces Decision-Based Hierarchical Learning (DBHL), a novel multi-sensor fire severity classification model that integrates Synthetic Aperture Radar (SAR; Sentinel-1 backscatter) and optical (Sentinel-2 reflectance) data. The model was applied to assess wildfire impacts on temperate forests during the 2019/20 “Black Summer” wildfire season in south-eastern Australia. DBHL incorporated SAR-based RADAR-Vegetation Structure Perpendicular Index (R-VSPI) and optical-based Vegetation Structure Perpendicular Index (VSPI) as candidate indices. By integrating these complementary datasets, DBHL leverages both structural and physiological changes as fire severity indicators, addressing limitations in single-sensor approaches. A pixel-wise approach was employed to spatially upscale the applicability of the R-VSPI and VSPI indices for fire severity assessment across the entire region. Using field data, the sensitivities of the R-VSPI and VSPI indices were validated during the immediate post-fire to one-year post-fire period. DBHL was trained and evaluated with a focus on comparing its performance against independent R-VSPI and VSPI classifications. The findings reveal the unique strengths of each index across various fire severity classes, demonstrating their complementary value. R-VSPI is more sensitive to structural changes in forests, while VSPI excels in identifying changes related to canopy-level disturbances. One-year post-fire recovery analysis shows distinct spatial patterns, with VSPI indicating faster recovery in surface vegetation and R-VSPI highlighting prolonged structural recovery. The DBHL model demonstrates the complementary strengths of the indices, allowing fire severity assessments to be contextualized across vertical vegetation strata, distinguishing between canopy-based damage indicators and underlying structural changes. DBHL outperformed single-sensor approaches, achieving the highest classification accuracy (overall accuracy=88.89%, kappa=0.86), particularly improving differentiation of Moderate (partial canopy scorch) and High (full crown scorch) severity with a producer’s accuracy of 100%, and 80%, respectively. Future research is aimed at integrating multi-wavelength SAR, including L-band (1.25 GHz) and P-band (0.43 GHz), along with LiDAR measurements to enhance structural fire severity assessments.

* Corresponding author.

E-mail address: aakash.chhabra7489@gmail.com (A. Chhabra).

<https://doi.org/10.1016/j.rse.2025.115163>

Received 4 April 2025; Received in revised form 19 August 2025; Accepted 23 November 2025

Available online 29 November 2025

0034-4257/© 2025 The Author(s). Published by Elsevier Inc. This is an open access article under the CC BY license (<http://creativecommons.org/licenses/by/4.0/>).

1. Introduction

Fire severity quantifies the loss or changes in aboveground and belowground organic matter due to wildfires and is a key component of wildfire regimes (Lentile et al., 2006; Keeley, 2009). It governs both immediate impacts (e.g., biomass consumption and tree mortality; Keeley, 2009) and long-term effects (e.g., vegetation regeneration and carbon storage dynamics; Morgan et al., 2014). Fire severity is influenced by wildfire intensity (Bradstock et al., 2010), forest age (Taylor et al., 2014), forest structure heterogeneity (Turner et al., 1999), seasonality (Miller et al., 2019), wildfire weather (Collins et al., 2019), topography, and vegetation type (Harris and Taylor, 2015). These factors drive variability in fire severity within a single wildfire, making wildfire behaviour complex and difficult to predict. In recent years, climate change has intensified wildfires globally, increasing their frequency, duration, and severity, causing substantial environmental and economic damage (Lozano et al., 2017; Littell et al., 2018; Vilà-Vilardell et al., 2020).

The 2019/2020 "Black Summer" wildfire season in south-eastern Australia was unprecedented in its extent and severity, reflecting a broader global trend of mega-wildfires and extreme wildfire seasons (Collins et al., 2021). Over 7.5 million hectares of forest burned between August 2019 and February 2020 (Boer et al., 2020; Davey and Sarre, 2020). Dry sclerophyll forests, dominated by eucalypts, were the most affected. While eucalypts are known for post-fire resprouting, the unprecedented scale and severity of these wildfires raise concerns about long-term ecosystem resilience (Le Breton et al., 2022).

Accurate fire severity mapping is critical for ecosystem recovery assessments, wildfire management, and long-term wildfire risk mitigation (Collins et al., 2014; Driscoll et al., 2024; Nolan et al., 2024; Quintero et al., 2025). However, mapping fire severity over such extensive areas requires consistent, large-scale, long-term datasets, which satellite remote sensing offers more cost-effectively than labor-intensive ground surveys (Engelbrecht et al., 2017; Chuvieco et al., 2020).

Wildfires alter the physical, chemical, and structural properties of vegetation, leading to noticeable differences in spectral and microwave properties (Tanase et al., 2010; Crowley et al., 2019). Traditional optical remote sensing has been widely used for fire severity assessments, that utilize the Normalized Burn Ratio (NBR) as a standard tool (Escuin et al., 2008; Veraverbeke et al., 2011, and Cardil et al., 2019). NBR makes use of the Near-Infrared (NIR) and Short-Wave Infrared (SWIR) bands, which are largely sensitive to variations in the chlorophyll and water content in vegetation (Chuvieco et al., 2006). In south-eastern Australia, operational fire severity mapping combines Sentinel-2 imagery with machine learning techniques like random forest models, complementing traditional methods like NBR (Gibson et al., 2020). However, NBR-based indices can be biased by green regrowth, making it difficult to distinguish between burned and unburned woody biomass (Roy et al., 2006). In contrast, reflectance in the SWIR band is influenced by both water content and woody biomass properties. To improve the consistency in post-fire measurements, Massetti et al. (2019) introduced the Vegetation Structure Perpendicular Index (VSPI). This index provides more consistent information on vegetation disturbance and recovery than traditional indices such as the NBR and Normalized Difference Vegetation Index (NDVI; Rouse Jr. et al., 1974). Despite these advantages, optical data is susceptible to factors such as vegetation phenology, smoke/cloud cover, and seasonal changes in sunlight reduce the ability to quantify fire severity, particularly with low severity burns or rapid vegetation regrowth (Tanase et al., 2013; Verbyla et al., 2008).

Synthetic Aperture Radar (SAR) overcomes optical limitations with its all-weather, day-and-night imaging capability (Le Toan et al., 1992; Ban et al., 2020), offering a reliable alternative for fire severity assessment, particularly in cloud-prone regions. SAR is sensitive to vegetation structure and soil moisture changes pre- and post-fire (Bourgeau-Chavez et al., 1997, 2007; Stroppiana et al., 2015). In radar imaging, burned

surface signatures vary with wavelength, polarization, fire severity, and environmental factors like soil moisture (Belenguer-Plomer et al., 2019). Vegetation loss reduces volumetric scattering, enhancing soil backscatter and increasing contrast between pre- and post-fire acquisitions (Reiche et al., 2015). Hence, SAR-based mapping of severity typically relies on the temporal difference between SAR backscatter data before and after a wildfire. Various SAR-based indices, including the Radar Vegetation Index (RVI) (Kim et al., 2011; Szigarski et al., 2018), the cross-to co-polarization ratio VH/VV (Vreugdenhil et al., 2018), Radar Burn Ratio (RBR_{SAR}) (Tanase et al., 2015b; Fernandez-Carrillo et al., 2019), and the Radar Forest Degradation Index (RFDI) (Mitchard et al., 2012; Saatchi, 2019), have been developed for post-fire assessments. More recently, Chhabra et al., 2022 introduced RADAR-VSPI (R-VSPI) as a SAR analogue to VSPI, demonstrating effectiveness in assessing wildfire-induced structure depletion and consistency in tracking the post-fire recovery, even during extended periods of cloud cover. Thus, the R-VSPI offers high-resolution insights into forest structure condition and heterogeneity, providing a valuable complement to traditional forest characterization methods and fire severity assessments (Chhabra et al., 2022). However, its complementarity with optical indices has not been fully explored.

In addition to empirical optical and SAR indices, physically based approaches have been applied to both sensing domains. For SAR, these include analyzing polarimetric decomposition responses at C- and L-bands (Tanase et al., 2013) or modeling frequency- and polarization-specific backscatter sensitivity to burn severity (Tanase et al., 2010), offering strong physical interpretability. For optical data, physically based radiative transfer models such as PROSAIL or LIBERTY (Jacquemoud et al., 2009; Verrelst et al., 2015), as well as a coupled canopy reflectance model used for Qinyuan pine fire severity (Yin et al., 2020), explicitly link spectral reflectance to vegetation structure and biochemical conditions. These approaches provide improved process understanding by explicitly linking sensor signals to vegetation biophysical parameters. However, both domains often require extensive ancillary data, site- and sensor-specific calibration, and large parameterization efforts and therefore best qualified for a long-term monitoring of specific wildfire-prone regions. However, their requirements limit their operational scalability in space and their near-real-time applicability for fire severity mapping (Baret and Buis, 2008).

Given the similar spatial and temporal resolutions of Sentinel-1 SAR and Sentinel-2 optical data (Zhang et al., 2019; Frantz et al., 2021), recent studies have explored SAR-optical fusion for improved fire severity classification (Hu et al., 2023). Methods such as fuzzy-set fusion (Stroppiana et al., 2015), regression-based feature-wise integration (Reiche et al., 2015), and deep learning models, such as U-Net (Zhang et al., 2021) and the more recent GAN-based SAR-to-optical translation (Hu et al., 2023) have been applied on spectral responses and SAR backscatter.

Despite advancements in SAR-optical fusion, significant limitations remain. Feature-extraction-based and deep learning models require extensive retraining with large historical datasets, making them computationally expensive and less generalizable across diverse landscapes, particularly for near real-time applications (Zhang et al., 2021; Belenguer-Plomer et al., 2021). Furthermore, fusion-generated optical images exhibit lower accuracy than real optical observations, particularly in heterogeneous landscapes. This highlights a fundamental challenge: SAR and optical datasets capture different physical properties, making it difficult to develop fusion algorithms that simplify effectively across ecosystems and wildfire regimes (Zhang et al., 2021). Therefore, no existing classification framework effectively integrates SAR and optical indices for fire severity mapping in Australia while remaining both interpretable and scalable for operational fire management. This gap is particularly concerning given the increasing frequency, extent, and severity of wildfires in temperate forests of south-eastern Australia (Bowman et al., 2020; Lindenmayer and Taylor, 2020).

Addressing these challenges, this study develops and validates a

novel, scalable supervised classification model, termed Decision-Based Hierarchical Learning (DBHL), to assess wildfire impacts on temperate forests from the 2019/20 “Black Summer” wildfire season in south-eastern Australia. The primary aim is to demonstrate the feasibility and workflow of the fused multi-sensor approach using DBHL, rather than to provide a statistically definitive assessment of its performance at the continental scale. The model integrates optical (Sentinel-2) and SAR (Sentinel-1) data, leveraging the complementary strengths of both observation types. The DBHL model employs the SAR-based R-VSPI and optical-based VSPI indices, which share a common mathematical foundation, ensuring a uniform approach to quantifying fire severity. The four key objectives are: (i) spatially upscale the applicability of R-VSPI and VSPI indices to cover entire landscape, (ii) validate these indices using extensive post-fire field survey data, (iii) train fire severity classifications using R-VSPI and VSPI separately, as well as through their integration within DBHL model, and (iv) assess and compare the performance of all three fire severity classification approaches.

2. SAR and optical index design

The R-VSPI and VSPI are SAR- and optical-based remote sensing metrics, respectively, designed to quantify disturbance-induced changes in forests relative to a baseline of healthy, undisturbed forests conditions from pre-disturbance period (Chhabra et al., 2022). Both indices share a common conceptual foundation, as their computation

rely on orthogonal transformations to measure the perpendicular deviation of an observed data point from a reference vegetation line in a two-dimensional spectral space (Fig. 1). The vegetation line, representing the pre-disturbance state of the forest, is defined by a simple linear function of the form: $y = mx + c$, where m is the slope, c is the intercept, and (x, y) represents the backscatter or the spectral response of undisturbed forest vegetation. The formulation of the vegetation line differs between SAR and optical data. For SAR, the radar vegetation line is derived from the linear relationship between co-polarized (VV) and cross-polarized (VH) backscatter (e.g., C-band, 5.4 GHz) (Chhabra et al., 2022) (Fig. 1B). In contrast, for optical data, the optical vegetation line is formed from the spectral response of SWIR bands (1.6 μm and 2.2 μm), following the approach of Massetti et al., 2019 (Fig. 1A). Although the radar and optical vegetation lines describe the pre-disturbance state of forest vegetation, they capture different physical properties. The radar vegetation line primarily reflects the structural integrity and biomass of the forest (Chhabra et al., 2022), whereas optical vegetation line is more sensitive to chemical composition changes such as biochemical properties, particularly cellulose and lignin content in woody vegetation (Curran, 1989; Massetti et al., 2019). However, when disturbances such

as wildfires occur, they alter the undisturbed forest state, shifting both the SAR backscatter response (Fig. 1B) and optical spectral reflectance (Fig. 1A) away from their respective pre-fire vegetation lines. Thus, R-VSPI and VSPI values for a given disturbed pixel are then computed as the perpendicular distance between its post-fire backscatter/reflectance and the vegetation line, using Equation 1 for R-VSPI and Equation 2 for VSPI (Chhabra et al., 2022).

$$R - VSPI_{pixels} = \frac{1}{\sqrt{m^2 + 1}} \times (VH_{pixels} - mVV_{pixels} - c) \quad (1)$$

$$VSPI_{pixels} = \frac{1}{\sqrt{m^2 + 1}} \times (SWIR2_{pixels} - mSWIR1_{pixels} - c) \quad (2)$$

Over time, the backscatter and surface reflectance values of disturbed vegetation gradually revert to their pre-disturbance state as vegetation recovers on ground (Fig. 1C).

3. Materials and methods

3.1. Study area

The study area encompasses the majority of the forest regions within the south-eastern Australian states Victoria (VIC), the Australian Capital Territory (ACT), and New South Wales (NSW) (Fig. 2). Six major bioregions are located in this part of Australia, each with unique climatic, geological, and forest vegetation characteristics as per the Interim Biogeographic Regionalization for Australia (IBRA, 2017). These include the Australian Alps, Brigalow Belt South, NSW North Coast, South East Corner, South Eastern Highlands, and Sydney Basin (Fig. 2). The primary vegetation types are woodlands and open forests with dry and wet eucalypt species of varying heights. Shorter trees (up to 10m) typically occupy upper slopes and ridges, while taller trees (20–30m) are found on lower slopes and in gullies (Collins et al., 2021). Shrublands, grasslands, and other vegetation types are also present but less common (Hutchinson et al., 2005). Forest areas were identified using a national spatial dataset based on the Australian forest definition, which specifies a mature height above 2m, and canopy cover over 20% (Australia’s State of the Forests Report, 2018). Data from these sources were compiled at 100m spatial resolution, and for this study, were resampled to a 10m pixel grid using the Albers Equal Area projection to match the Sentinel-1 data. The 2019/20 “Black Summer” wildfires’ timeline showcased distinct variations in their onset and peak (Fig. 2). The initial wildfires ignited in northern NSW as early as August 2019 (southern hemisphere late winter) and gradually commenced further south over the succeeding 5-7 months (Bowman et al., 2021; Nolan et al., 2021). Fig. 2 outlines

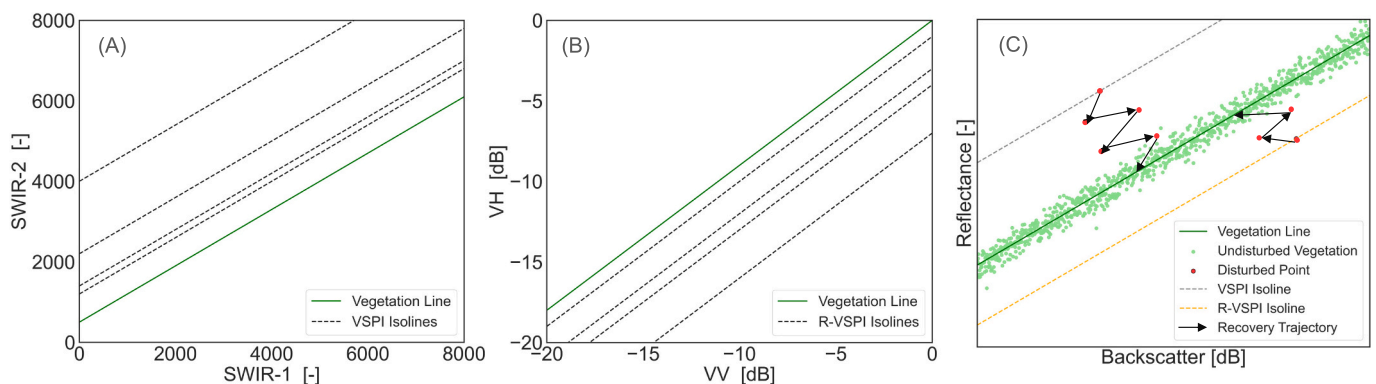


Fig. 1. Illustration of (A) VSPI in the optical domain and (B) R-VSPI in the SAR domain. The solid green line represents healthy vegetation, while the dashed isolines indicate the orthogonally displaced vegetation state due to external disturbances such as wildfires. Optical values from SWIR-2 and SWIR-1 bands are expressed as surface reflectance in linear units, whereas SAR backscatter from VH and VV polarization channels are expressed in decibels [dB]. (C) Schematic representation of vegetation disturbance and recovery, where green dots along the solid green line indicate undisturbed vegetation, and red dots represent post-fire disturbance, progressing from dashed isoline of the optical (gray) and SAR (orange) towards the vegetation line. Figs 1A and 1C are adapted from Massetti et al. (2019), and Fig 1B is adapted from Chhabra et al. (2022)

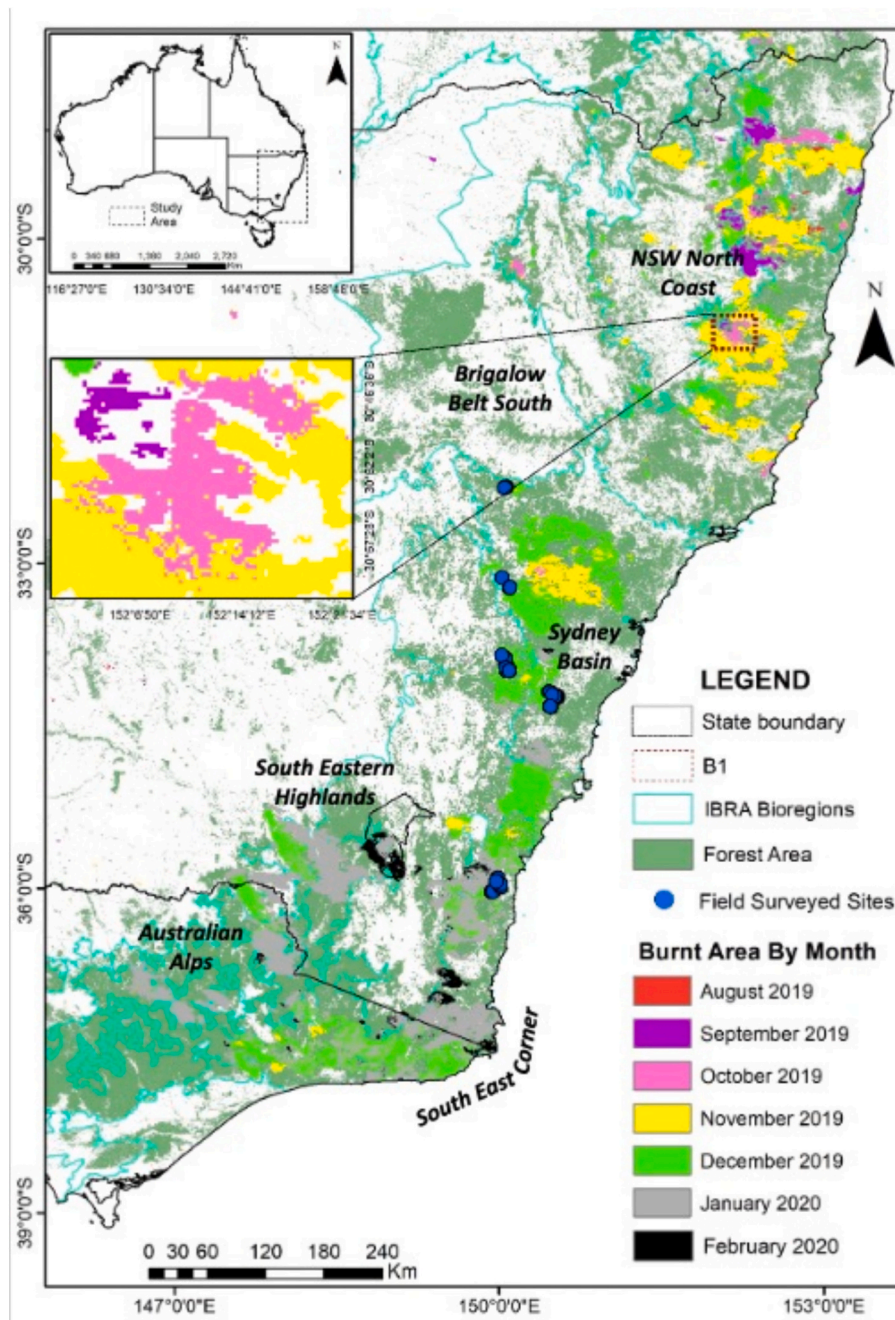


Fig. 2. Study area in south-eastern Australia depicting the forest regions cover (green), the six bioregions (delineated by blue boundaries), temporal progression of the wildfire-affected areas throughout south-eastern Australia during the 2019/2020 "Black Summer" wildfire season, and the field sites (blue dots) utilized for validation purposes. The monthly burnt area data was obtained from MODIS MCD64A1 – Collection 6 product (Giglio et al., 2018). The inset map B1 offers a closer view of the Oxley Wild Rivers National Park in NSW, a study site affected by 2019 wildfires in September (purple), October (pink) and November (yellow). The delineation of forest areas was informed by the national forest extent map (Montreal Process Implementation Group for Australia and National Forest Inventory Steering Committee, 2018). The demarcation of the bioregions was accomplished using the boundary extents derived from shapefiles (IBRA, 2017).






the wildfire progression using the MODIS burned area product (MCD64A1 – Collection 6), which records daily global burned areas at 500m resolution (Giglio et al., 2018). To align with the Sentinel-1 satellite data, the MODIS data at a 500m resolution were also resampled to a uniform 10m pixel grid using an Albers Equal Area projection and using a nearest-neighbor approach.

3.2. Post-fire field survey sites and fire severity assessment

Field surveys were conducted approximately one-year after the 2019/20 wildfires to assess their impact (Nolan et al., 2022; indicated by

blue dots in Fig. 2). A total of 60 plots were sampled across multiple forest types: 45 in in the Blue Mountains and 15 in South Coast between October and December 2020. Plot size and layout varied by region. In the Blue Mountains and South Coast, each plot comprised two 45m orthogonal transects (north-south, east-west). All trees ≥ 2.5 cm DBH were measured within 5m of one side of one transect, and all trees ≥ 20 cm DBH were measured within 5m of both sides of both transects. Fire severity at each plot was classified based on the extent of vegetation scorching and the consumption of canopy and understory layers by the wildfire, with distinctions made along a gradient of severity levels (Table 1). The 'Unburnt' and 'Low' severity classifications represent

Table 1
Fire severity classification and definitions.

Severity Class	Definition	% foliage wildfire affected	Pixel Colour
Unburnt	Unburnt	0% canopy and understorey burnt	
Low	Burnt surface with unburnt canopy	>10% burnt understorey / > 90% green canopy	
Moderate	Partial canopy scorch	20–90% canopy scorch	
High	Full canopy scorch (+/- partial canopy consumption)	>90% canopy scorch / 50% canopy biomass consumed	
Extreme	Full canopy consumption	>50% canopy biomass consumed	

surface-level impact, whereas ‘Moderate’, ‘High’, and ‘Extreme’ classifications correspond to canopy-level severities. Table 2 summarizes the vegetation types in the field survey sites, as classified by Keith (2004). Distribution of fire severity classes varied among plots, with low and extreme severities less commonly observed within the same forest type (Gibson et al., 2022).

3.3. SAR and optical satellite-data acquisition and aggregation

Copernicus Sentinel-1 C-band (5.4 GHz) dual-polarization radar data were utilized, collecting vertical-vertical (VV) and vertical-horizontal (VH) polarizations in Interferometric Wide (IW) swath mode (Torres et al., 2012). A time series from January 1, 2017, to August 30, 2019, was compiled from Google Earth Engine (GEE; Gorelick et al., 2017), with overpasses occurring every 12 days (same orbit) over south-eastern Australia, as only Sentinel-1A was continuously operational during this period. The dataset includes SAR-Ground Range Detected (GRD) scenes which were pre-processed to correct for thermal noise, radiometric calibration, and terrain (Gorelick et al., 2017), resulting in a calibrated and orthorectified COPERNICUS/S1_GRD product with normalized backscatter coefficients in dB scale. Further speckle reduction was achieved for this study using a sliding 11x11 pixel-window linear averaging technique, leading to an effective resolution of 110m while retaining a 10m pixel spacing. The primary motivations behind choosing this method were twofold. Firstly, to maintain a large number of pixels for estimating the reference vegetation line to ensure a statistically more stable retrieval. This also ensured reduced noise levels and a better capture of the dynamic behavior of the local vegetation. Secondly, it was designed to retain pixel-level variability and sub-pixel heterogeneity, to enable the detection of variations and patterns within the vegetation at higher resolution. This aggregation method is expected to provide an accurate representation of the spatial variability inherent in forest structure while reducing speckle noise in the SAR data.

The Sentinel-2 Level-2A (L2A) data used in this study are the GEE-provided data which come as orthorectified and atmospherically corrected surface reflectance (COPERNICUS/S2_SR) and covered the period

Table 2
Distribution of field sites across regions, wildfires, vegetation communities, and fire severity classes (Nolan et al., 2022).

Region	Vegetation Community (Keith, 2004)	Wildfire Name	Fire Severity Class					Total
			Unburnt	Low	Moderate	High	Extreme	
Blue Mountains	Wet Sclerophyll Forest	Green Wattle Creek	3	3	4	4	1	15
Blue Mountains	Sydney Hinterland Dry Sclerophyll Forest	Green Wattle Creek	3	2	3	4	3	15
Blue Mountains		Meads Creek West	2	1	2	1	2	8
Blue Mountains	Western Slopes Dry Sclerophyll Forest	Owens Creek	1	1	0	3	2	7
South Coast	South Coast Dry Sclerophyll Forest	Badja Forest Rd	3	4	3	4	1	15

from January 1, 2017, to August 30, 2019, at the time this study was undertaken. For this study, the data were further post-processed as follows. Surface reflectance acquisitions from SWIR1 (Band11: 1.56-1.66 μm) and SWIR2 (Band12: 2.11-2.29 μm) channels were extracted from cloud-free (<20% cloud cover) Sentinel-2 acquisitions (Drusch et al., 2012). The data were filtered to exclude snow, water, cirrus, and cloud shadows using a quality assessment band (Gorelick et al., 2017) and resampled to match the spatial resolution of Sentinel-1 (10m) using a nearest neighbor approach.

3.4. Large-scale analysis of wildfire events

To enable large-scale spatial analysis of fire severity and post-fire conditions in south-eastern Australian Eucalypt forests, a pixel-wise linear regression was applied between two pairs of bands: Sentinel-1 (VV and VH) and Sentinel-2 (SWIR1 and SWIR2), following the methodology outlined in section 2. The analysis used pre-fire data from January 1, 2017, to August 30, 2019, for Sentinel-1 and from January 1, 2017, to August 30, 2019, for Sentinel-2. The August 2019 cut-off ensured the data represented the (baseline) vegetation state leading up to the large-scale wildfire events of the 2019/20 wildfire season. The derived regression slopes and offsets were assessed for spatial variations across the study area, allowing for a more detailed analysis of the variability in vegetation response across different regions. These regression parameters were also then used to compute R-VSPI and VSPI from the equations outlined in section 2. The indices were computed for three different periods (i.e., pre-, immediate-, and one-year post-fire), to present a sequence of changes in forest vegetation in south-eastern Australia. For each of the three analysis periods i.e., pre-fire, immediate post-fire, and one-year post-fire, the spatial maps were produced from the monthly time composites from all available Sentinel-1 and Sentinel-2 scenes corresponding to the month of the acquired acquisition date. This ensured seasonal consistency between periods and reduced short-term variability caused by different wildfire dates. Median compositing was applied to suppress outliers, minimize Sentinel-1 speckle, reduce Sentinel-2 cloud/shadow effects, and fill temporal data gaps, while retaining key spectral and backscatter signal characteristics. Since the soil and vegetation moisture strongly influence SAR backscatter and can obscure wildfire-induced structural changes (Belenguer-Plomer et al., 2019), Sentinel-1 acquisitions for all three periods were carefully screened to avoid dates immediately following rainfall. Daily precipitation records (Australian Bureau of Meteorology (BoM), n.d) were checked, confirming that no significant rainfall occurred around the selected acquisition dates.

3.5. Statistical analysis

Violin plots were generated to illustrate R-VSPI and VSPI values for a total of 60 field survey sites, each representing a unique location where fire severity was surveyed in the field and matched to coincident satellite-derived index values. These sites were classified into five fire severity classes from two distinct time stamps: immediate-post-fire (R-VSPI-February 28, 2020; VSPI-February 26, 2020) and one-year post-

fire (R-VSPI-September 16, 2021; VSPI-September 18, 2021). To define the index ranges for each severity category, values from the field-surveyed dataset were filtered to the 95th and 5th percentiles to minimize the influence of statistical outliers (e.g., from sensor noise, local anomalies, or atypical conditions) and to improve class separability. This percentile filtering was applied only to the training dataset whereas the complete index range was retained when generating the final classification maps to ensure that all potentially burned pixels were evaluated. With severity classifications established for both indices, the study aimed to provide a series of spatially explicit post-fire observations for the entire forest region of south-eastern Australia.

3.6. Fire severity model development and accuracy assessment

3.6.1. Independent fire severity classification

The wall-to-wall independent fire severity classification was conducted separately for the R-VSPI and VSPI indices, and maps were

generated for the immediate post-fire image. Each index was processed independently to preserve its unique sensitivity to wildfire impacts across the south-eastern Australian Eucalypt forests. The independent classification from each index was achieved by applying the severity thresholds for each class, as established in Section 3.5. These thresholds were applied per pixel to the immediate post-fire raster, assigning each pixel to one of five discrete severity classes ('Unburnt', 'Low', 'Moderate', 'High', 'Extreme') as defined in Table 1.

3.6.2. Development of Decision-Based Hierarchical Logic (DBHL) fire severity classification model

Following the independent fire severity classification, a supervised classification model, DBHL, was developed that integrate both R-VSPI and VSPI into a unified framework, to assess wildfire impacts across the south-eastern Australian Eucalypt forests. The DBHL model operates through a tiered decision process based on the severity thresholds for each class in both indices, as established in Section 3.5. These thresholds

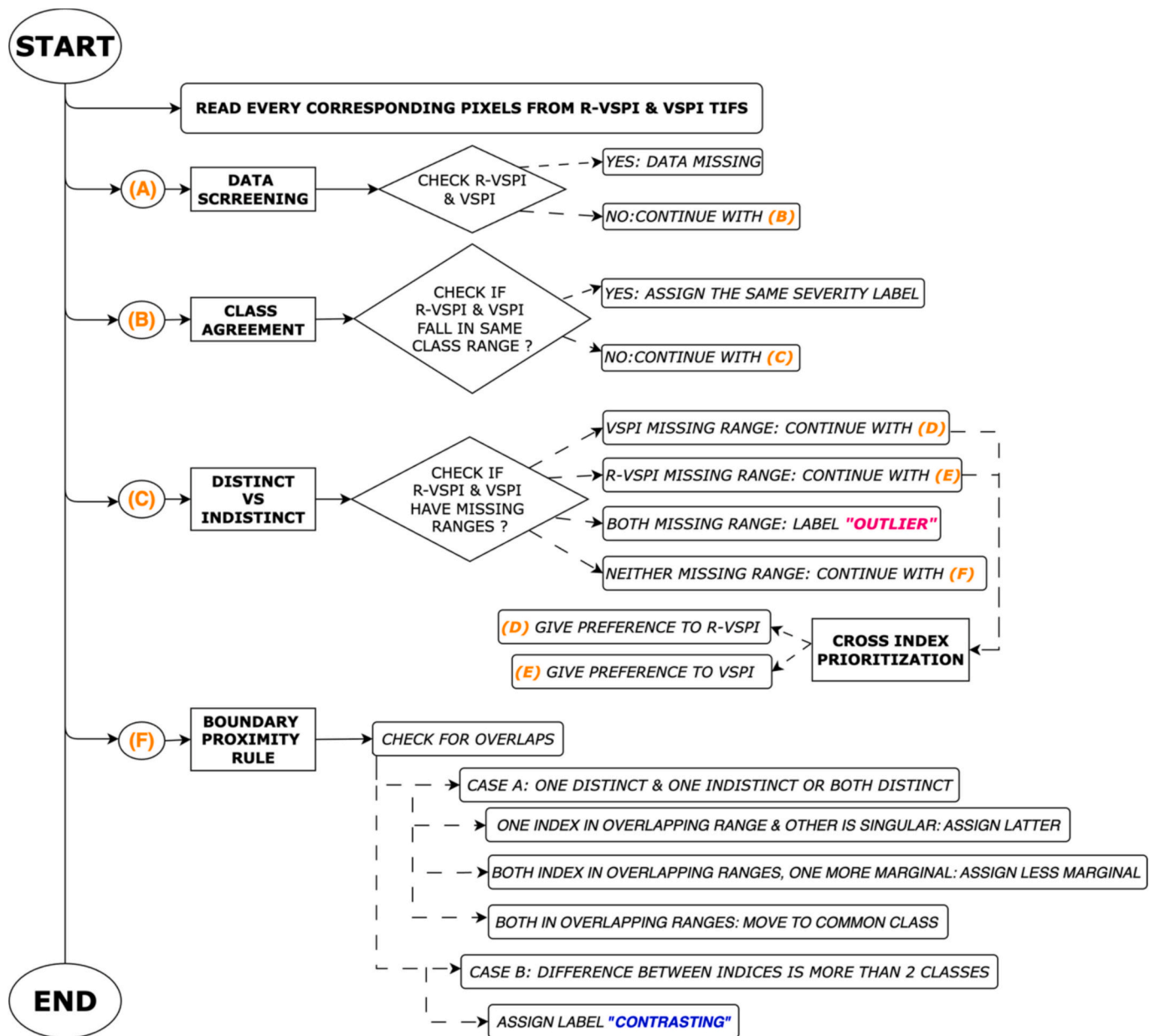


Fig. 3. Schematic representation of the workflow for the Decision-Based Hierarchical Learning (DBHL) classification algorithm for fire severity classification using R-VSPI and VSPI.

were applied per pixel to the immediate post-fire raster, assigning each pixel to one of five discrete severity classes ('Unburnt', 'Low', 'Moderate', 'High', 'Extreme') as defined in Table 1.

Fig. 3 illustrates the DBHL model for fire severity classification. The DBHL steps were designed to systematically resolve classification ambiguities while capitalizing on the complementary sensitivities of R-VSPI and VSPI in fire severity mapping while also minimizing errors caused by sensor-specific limitations. For each pixel, values from the composed immediate post-fire R-VSPI and VSPI raster were processed sequentially through a defined set of steps (Fig. 3). Data Screening is involved as the first to check both indices for valid values. This ensured that noise or artefacts did not influence the results. Pixels with missing values in both indices were assigned a 'No Data' label and excluded. If only one index was missing, the valid index proceeded to the next step. Class Agreement then followed where both indices returned the same severity class (as defined in Table 1), that class was directly assigned. This allowed for rapid and reliable classification where both sensors concurred, increasing confidence in those outputs. If the classes differed, then Distinct vs. Indistinct Ranges were evaluated. In this step, if only one index produced a valid severity range, Cross-Index Prioritization was applied which assigned the R-VSPI class when VSPI was missing, and the VSPI class when R-VSPI was missing. This preserved spatial coverage by reducing gaps caused by atmospheric interference or other acquisition limitations. Pixels where both indices lacked distinct ranges were labelled 'Outlier' and excluded. When both indices returned valid but non-matching classes, their proximity to class boundaries were examined by the Boundary Proximity Rule. If one index was in an overlapping boundary range and the other index in a singular range, the singular class was chosen. If both indices were in overlapping ranges but one was marginally closer to a neighboring class, the less marginal value was selected. If both indices were in overlapping ranges without a clear marginal difference, the common overlapping class was assigned. These rules reduced random misclassifications by resolving marginal threshold cases. Finally, if the difference between indices exceeded two class levels, the pixel was labelled 'Contrasting' to flag substantial disagreement.

3.6.3. Model training, validation and accuracy assessment

The classification model was trained and validated using 60 data points from a spatially explicit, field-validated fire severity dataset collected across multiple wildfires in the study region (Fig. 1, Table 2). Points were selected using a stratified random sampling approach to ensure balanced representation across all five severity classes and major vegetation types, while maintaining adequate spatial separation between points to minimize redundancy due to spatial autocorrelation. The dataset was split 70:30 into 42 training points and 18 validation points. While the training subset averaged ~8 points per class, the supervised rule construction was informed by severity class boundaries established from the full field dataset, ensuring representativeness across sites and conditions. The 42 training points are shown in the violin plots to illustrate their distribution within each severity class. For all three classifications, response variables were defined as fire severity classes: 'Unburnt', 'Low', 'Moderate', 'High', and 'Extreme', while predictor variables included R-VSPI and VSPI values. Model training and predictions were undertaken using the Scikit-learn package in Python (Pedregosa et al., 2011). Fire severity classification models were systematically evaluated by comparing the performance of individual predictors (R-VSPI and VSPI) and their combined implementation within DBHL. The model's accuracy was assessed using field-validated severity classifications to quantify its ability to differentiate fire severity across wildfire-affected regions. The validation data consisted of a full sampling dataset from the target wildfire, ensuring complete independence from training data. Classification accuracy was primarily assessed using overall accuracy (OA), producer accuracy (PA), and user accuracy (UA) (Congalton and Green, 2019). Additionally, the Kappa statistic was employed to evaluate the statistical agreement between

model predictions and validation data, and to compare the relative performance of different classifications (Story and Congalton, 1986). Models with Kappa values >0.75 are generally considered excellent, while those <0.4 are regarded as poor (Allouche et al., 2006).

4. Results

4.1. Spatial-temporal dynamics of forest disturbance and recovery

Figs. 4 and 5 present a sequence of changes in forest vegetation in south-eastern Australia, captured by the R-VSPI and VSPI time composites for three periods: (A) pre-fire (August 2019), (B) immediate post-fire (February 2020), and (C) one-year post-fire (September 2021) conditions. Before the wildfire, the R-VSPI derived pre-fire condition map (Fig. 4A) primarily exhibits widespread areas with neutral to slightly positive decibel values (green). Similarly, the VSPI map (Fig. 5A) shows low values (green) across south-eastern Australia. However, immediate post-fire conditions show a marked decline in R-VSPI values, with extensive regions particularly in the southern and coastal regions displaying strong negative decibel values (red) (Fig. 4B). The VSPI map similarly indicates substantial wildfire-induced change, with a pronounced increase in VSPI values (red) along the south-eastern coastline (Fig. 5B). One-year post-fire patterns differ between the two indices. The R-VSPI map shows signs of recovery, with many areas transitioning back toward neutral decibel values (yellow to green) particularly in moderately burned regions. However, some high severity burned regions remain degraded retaining persistently low R-VSPI decibel values (Fig. 4C). In contrast, the VSPI map (Fig. 4C) shows a decline in VSPI values (yellow to green) compared to the immediate post-fire period. This pattern is most pronounced in the northern and inland regions (Fig. 5C).

4.2. Independent and joint fire severity classification schemes across south-eastern Australia

4.2.1. Evaluation of R-VSPI and VSPI sensitivities against field-observed fire severity

Fig. 6 presents violin plots illustrating the distribution of (A) R-VSPI and (B) VSPI values across five different fire severity classes for field sites during two post-fire time periods: immediate-post-fire (blue) and one-year post-fire (orange). The plots illustrate the variability and central tendency of R-VSPI and VSPI, highlighting distinct shifts between the immediate-post-fire and one-year post-fire periods. The R-VSPI values decrease (become more negative) with increasing fire severity immediately after the wildfire (Fig. 6A). 'Unburnt' severity exhibits a narrow distribution with values centered around -0.5 dB, while 'Low' to 'Extreme' severity classes display progressively lower

R-VSPI values, reaching below -2.0 dB in extreme burn areas. One-year after the fire, R-VSPI values across all severity classes shift toward less negative values, with notable increases in 'Moderate', 'High', and 'Extreme' severity regions. The largest shift is observed in 'Extreme' severity, where the post-fire distribution narrows and moves closer to pre-fire conditions (Fig. 6A).

In VSPI (Fig. 6B), immediate post-fire values show a strong positive relationship with fire severity, with 'Unburnt' and 'Low' severity displaying relatively low VSPI values, while 'High' and 'Extreme' severity peaks above 600. One-year after the wildfire, VSPI values decrease across all severity classes, with the greatest reductions in 'High' and 'Extreme' severities. The spread of VSPI distributions also contracts over time toward post-fire stabilization, particularly in 'Moderate' and 'High' severities (Fig. 6B).

4.2.2. Spatial patterns of R-VSPI, VSPI and DBHL fire severity classifications

Table 3 outlines the fire severity class ranges for R-VSPI and VSPI, derived from the 95th and 5th percentiles of each field-validated

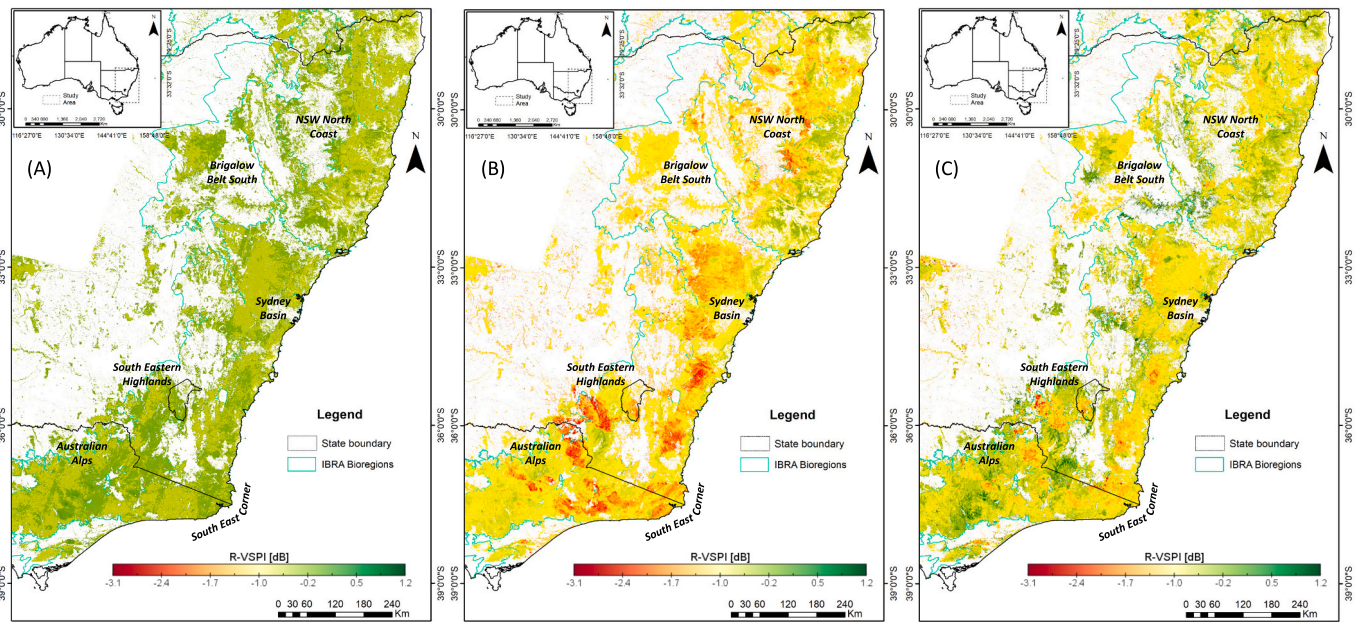


Fig. 4. Temporal evolution of forest vegetation across south-eastern Australia as depicted by Sentinel-1-derived R-VSPI maps encompassing six different bioregions. The images highlight three key stages of forest health: (A) pre-fire undisturbed vegetation (August 2019), (B) immediate post-fire wildfire-affected vegetation (February 2020), and (C) one-year post-fire recovery (September 2021). The images used for R-VSPI were acquired and composited to depict the aforementioned periods effectively. The R-VSPI values portray the degree of forest disturbance and recovery, where negative values indicate a disturbance level and positive values or near zero values represent an undisturbed state or the progress of post-disturbance recovery.

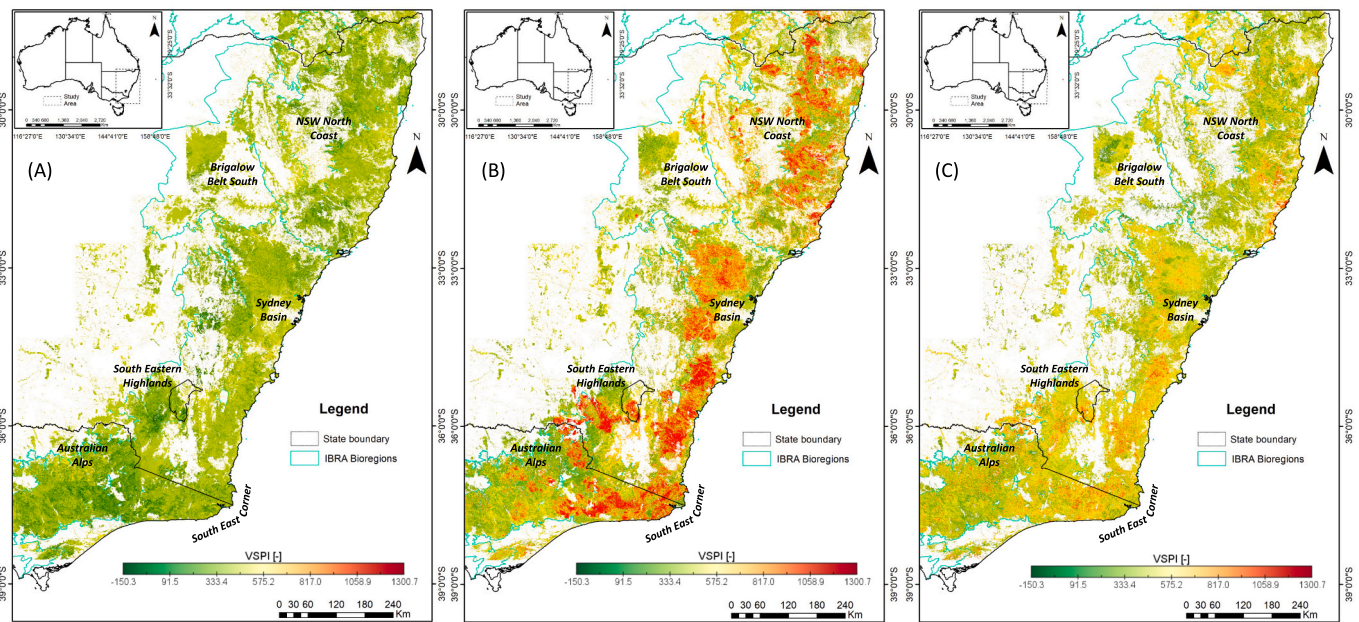


Fig. 5. Temporal evolution of forest vegetation across south-eastern Australia as depicted by Sentinel-2-derived VSPI maps encompassing six different bioregions. The images highlight three key stages of forest health: (A) pre-fire undisturbed vegetation (August 2019), (B) immediate post-fire wildfire-affected vegetation (February 2020), and (C) one-year post-fire recovery (September 2021). The images used for VSPI were acquired and composited to depict the aforementioned periods effectively. The VSPI values portray the degree of forest disturbance and recovery, where positive values indicate a disturbance level and negative values or near zero values represent an undisturbed state or the progress of post-disturbance recovery.

severity category shown in Fig. 6. With this information, a combined fire severity supervised classification algorithm DBHL is proposed, allowing a systematic and consistent combined index across space and time (Fig. 3).

Fig. 7 display the spatial distributions of fire severity classifications across south-eastern Australia ranging from ‘Unburnt’ to ‘Extreme’ as

defined in Table 1. The classifications are based on three different approaches, R-VSPI-based classification (Fig. 7A), derived from Sentinel-1 SAR backscatter; VSPI-based classification (Fig. 7B), sourced from Sentinel-2 optical reflectance; and DBHL classification (Fig. 7C), which integrates R-VSPI and VSPI for a combined severity assessment. The images used for the R-VSPI and VSPI classifications were acquired and

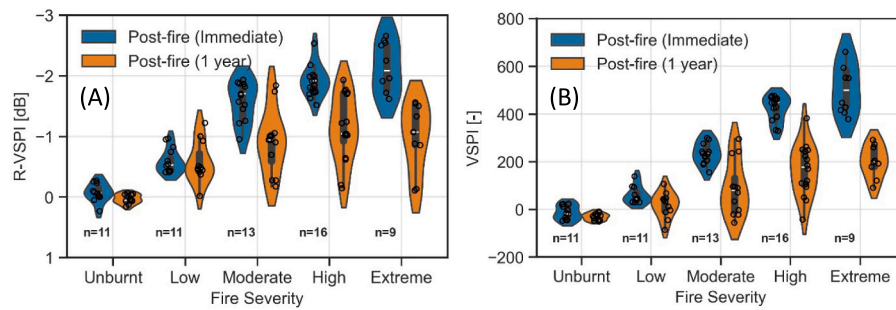


Fig. 6. Violin plots illustrating (A) R-VSPI and (B) VSPI values across fire severity classes for two different time stamps: immediate post-fire (blue) and 1-year post-fire (orange). The label n denotes the number of data points per severity class which is the same for both time stamps. Individual data points are shown as circular dots.

Table 3

Calculated ranges of R-VSPI and VSPI for five fire severity classes based on 95th and 5th percentiles.

Fire Severity	R-VSPI [dB]	VSPI [-]
Unburnt	(0.234) to (-0.267)	-46.965 to 41.748
Low	(-0.380) to (-0.964)	29.658 to 129.860
Moderate	(-0.951) to (-2.36)	172.857 to 296.038
High	(-1.215) to (-2.533)	265.944 to 473.502
Extreme	(-1.480) to (-2.995)	397.879 to 1150.14

composed for a date at the end of the main wildfire season 2019/20 (February 28, 2020). Fig. 7A shows R-VSPI-based classification and highlights ‘High’ (red) to ‘Extreme’ (black) fire severity predominantly in the southern bioregions, including the South East Corner, Australian Alps, and South Eastern Highlands. These areas exhibit concentrated patches of severe wildfire impact, with ‘Moderate’ (orange) severity forming a buffer around these ‘High’ severity zones. The R-VSPI based classification also shows less extensive ‘High’ severity burns in the Sydney Basin, Brigalow Belt South, and NSW North Coast, where ‘Low’ (yellow) and ‘Unburnt’ (green) severities dominate. In these regions, the classification shows more spatial fragmentation, with isolated patches of

‘Moderate’-to- ‘High’ severity interspersed within largely ‘Unburnt’ severity. Fig. 7B, based on VSPI, reveals a more widespread spatial extent of fire severity compared to R-VSPI. Areas classified as ‘High’ and ‘Extreme’ severity cover larger continuous landscapes, particularly across the NSW North Coast, Brigalow Belt South, and Sydney Basin, which show extensive red and black regions. In the southern bioregions (Australian Alps, South Eastern Highlands, and South East Corner), the fire severity patterns remain largely consistent with the R-VSPI map, with concentrated ‘Extreme’ (black) severity and surrounding ‘Moderate’ (orange) severity. Notably, the ‘Low’ (yellow) and ‘Moderate’ (orange) severity classifications are more extensively distributed, forming broader transition zones between fire severity levels, rather than the more localized patches seen in R-VSPI. In contrast to R-VSPI, the VSPI-based classification captures a more extensive footprint of burnt areas in the central and northern regions, highlighting that optical-based indices may detect wildfire-affected vegetation beyond what is apparent in SAR backscatter.

Fig. 7C presents the DBHL model’s integrated classification where southern bioregions (Australian Alps, South Eastern Highlands, and South East Corner) remain the most wildfire-affected regions, retaining large patches of ‘Extreme’ (black) and ‘High’ (red) severity classifications. Further north, the DBHL classification reconciles discrepancies

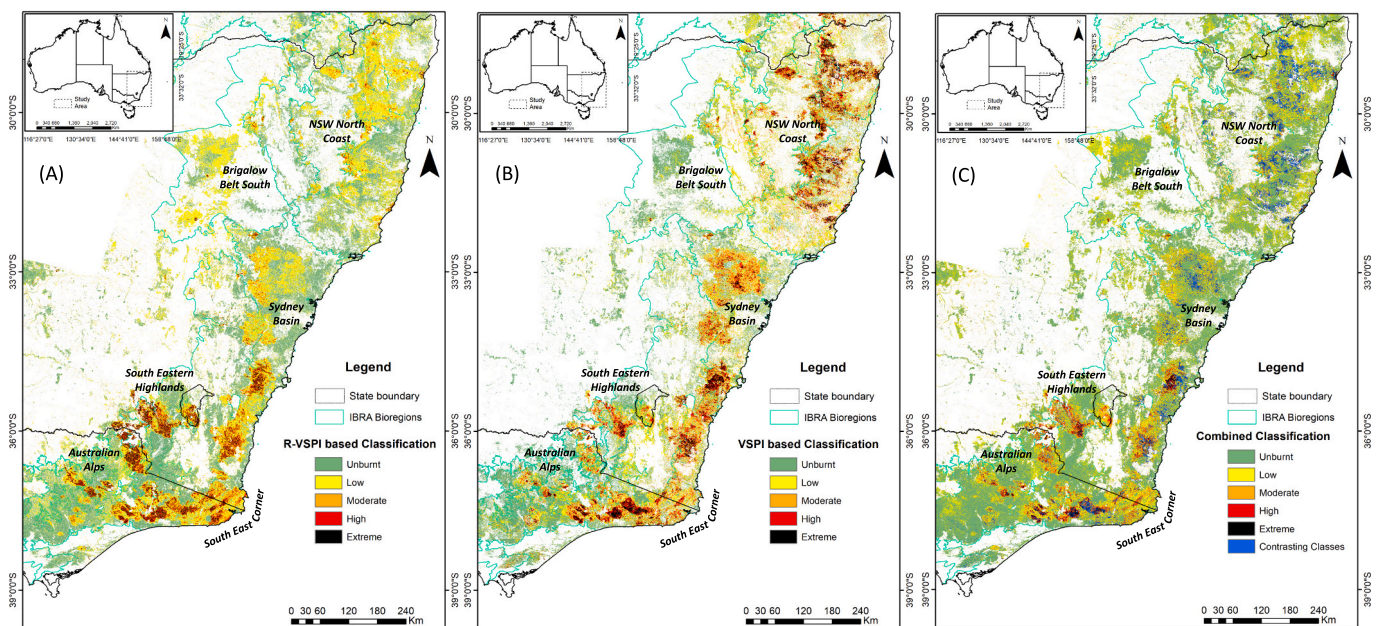


Fig. 7. Examples of burnt area extent and fire severity classification maps: (A) Fire severity classification derived from Sentinel-1-based R-VSPI; (B) Fire severity classification sourced from a Sentinel-2-based VSPI; and (C) Decision-based combined classification from the integration of independent R-VSPI and VSPI classifications. The images used for the R-VSPI and VSPI classifications were acquired and composited over the immediate post-fire period (February 2020). The fire severity classes used are in line with those described in Table 1.

between R-VSPI and VSPI in the Sydney Basin, Brigalow Belt South, and NSW North Coast, where VSPI mapped more ‘Extreme’ and ‘High’ severity levels, while R-VSPI classified this as ‘Low’ severity. The ‘Contrasting’ regions (blue-colored pixels areas in Fig. 7C), concentrated in Brigalow Belt South and NSW North Coast, mark zones of localized divergence between the SAR and optical-based indices.

4.2.3. Accuracy assessment of independent and joint fire severity classification models

Fig. 8 shows a comparative evaluation of the three fire severity classification models—R-VSPI, VSPI, and DBHL. The R-VSPI-based classification achieved an OA=66.67%, with a kappa statistic of 0.5814. The confusion matrix (Fig. 8A) shows that ‘Unburnt’ and ‘Low’ severity areas were classified with high accuracy (PA=100%, UA=100%), whereas ‘Moderate’, ‘High’, and ‘Extreme’ severity classes exhibited higher misclassification rates. For ‘Moderate’ severity, 66.67% were correctly classified (PA=66.67%), while 33.33% were misclassified into ‘High’ severity (UA=33.33%).

Similarly, ‘High’ severity had a PA of 60%, with 40% misclassified into ‘Moderate’ severity. Notably, ‘Extreme’ severity was entirely misclassified (PA=0%), with this severity predominantly assigned to ‘Moderate’ and ‘High’ severity categories. The VSPI-based classification achieved a higher OA=72.22%, with a kappa statistic of 0.659, demonstrating an improvement over R-VSPI. The confusion matrix in Fig. 8B shows that ‘Moderate’ and ‘Extreme’ severities were more accurately classified compared to R-VSPI, but misclassification persisted in distinguishing ‘Unburnt’ and ‘Low’ severity areas. For ‘Extreme’ severity, PA=100%, meaning all ‘Extreme’ severity classes were correctly identified. However, ‘Unburnt’ severity had a PA=50%, with 50% misclassified as ‘Low’ severity. Similarly, ‘High’ severity had a PA=40%, with 60% misclassified into ‘Moderate’ severity. Additionally, ‘Moderate’ severity was classified with PA=100%, though 50% were misclassified as ‘Low’ severity.

The DBHL classification model demonstrated the highest OA=88.89%, with a kappa statistic of 0.862. The confusion matrix for DBHL (Fig. 8C) shows that all severity classes were classified with improved accuracy compared to independent classifications from R-VSPI and VSPI, particularly in ‘Moderate’ and ‘Extreme’ severity, where misclassifications were minimized. For ‘Moderate’ severity, PA improved to 100%, ensuring that no misclassifications occurred in this category. ‘High’ severity had a PA of 80%, an increase from both R-VSPI and VSPI classifications. ‘Extreme’ severity, which were misclassified entirely by R-VSPI and partially by VSPI, were now classified with a PA of 66.67%. An additional category, ‘Contrasting’, was introduced in DBHL to represent areas where R-VSPI and VSPI classifications diverged significantly. The confusion matrix shows some ‘Extreme’ severities

were classified as ‘Contrasting’ (33.33%).

5. Discussion

5.1. Complementary sensitivity of R-VSPI and VSPI across south-eastern Australia

The observations in Figs. 4 and 5 highlight key divergent sensitivities of SAR and optical data in south-eastern Australian forests, showing how R-VSPI and VSPI respond differently to (A) pre-fire (August 2019), (B) immediate post-fire (February 2020), and (C) one-year post-fire (September 2021).

5.1.1. R-VSPI sensitivity across pre-fire, immediate post-fire, and one-year post-fire

The neutral to slightly positive R-VSPI values in Fig 4A, derived from Sentinel-1 backscatter, indicate a structurally intact and undisturbed forest. The dominance of volumetric scattering was not directly measured but inferred based on established C-band SAR scattering theory and the relative sensitivity of VH polarization to canopy foliage and fine branch structures (Ulaby and Long, 2014). This consistent pattern across the landscape confirms the absence of significant structural disturbances prior to the wildfire (Engelbrecht et al., 2017; Tanase et al., 2010). Fig 4B show a sharp decline in the R-VSPI values as compared to the values in the pre-fire state. This reduction reflects a loss of volumetric scattering linked to canopy foliage and fine branches. At the same time, decreases observed in both VV and VH channels point to a relative increase in surface scattering, consistent with greater ground exposure after canopy and understory consumption (Tanase et al., 2010; Fernández-Guisuraga et al., 2022). This suggests that R-VSPI is particularly effective in identifying high-severity burn areas where tree mortality and structural loss are dominant (Chhabra et al., 2022). However, in some regions, R-VSPI remains relatively stable despite wildfire occurrence, suggesting that while surface vegetation may have burned, larger structural components such as trunks and branches persisted, limiting drastic changes in SAR backscatter (Le Toan et al., 1992; Tanase et al., 2018). Double-bounce scattering, which may theoretically arise from trunk-ground interactions in such cases, was not quantified here because Sentinel-1 provides only dual polarization (VV, VH), which prevents full polarimetric decomposition. Moreover, at C-band, canopy penetration is shallow, limiting sensitivity to trunk-ground interactions unless canopy stripping is extreme (Cloude and Pottier, 2002; Navarro-Sanchez et al., 2013).

R-VSPI trends toward neutral values in moderately burned areas, reflecting gradual structural recovery (Fig. 4C). However, regions affected by severe canopy loss continue to exhibit persistently low R-

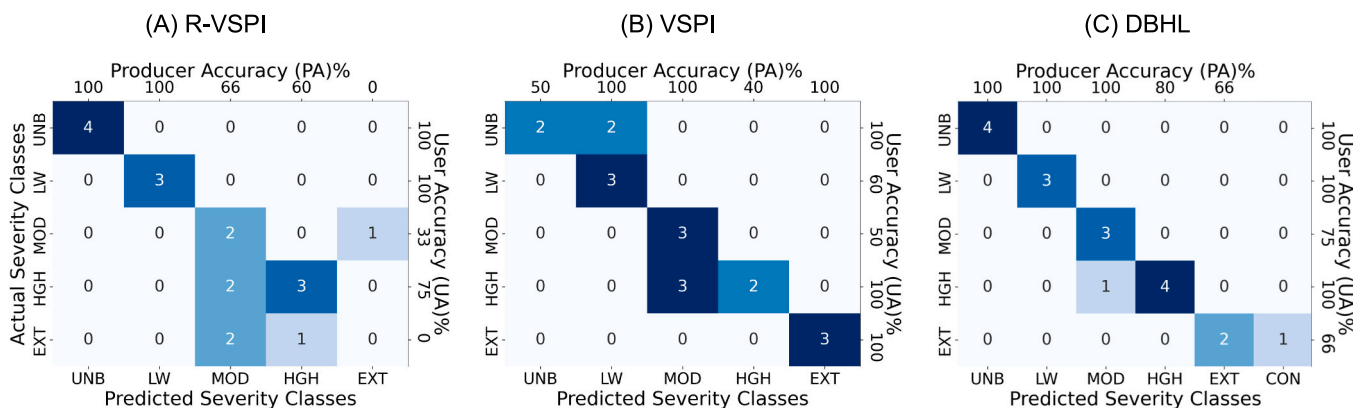


Fig. 8. Confusion matrices for three fire severity classification approaches: (A) R-VSPI, (B) VSPI, and (C) DBHL. The intensity of the color corresponds to the number of correctly and incorrectly classified severity instances. The matrices display the classification performance across severity classes, with the actual fire severity on the y-axis and predicted severity on the x-axis. Producer’s Accuracy (PA) and User’s Accuracy (UA) percentages are shown, indicating the reliability of each classification model. Severity class acronyms: UNB=Unburnt, LW=Low, MOD=Moderate, HGH= High, EXT=Extreme, CON=Contrasting.

VSPI values, indicating that full forest regrowth has not yet occurred. Since SAR backscatter is influenced by woody biomass and vertical structure, R-VSPI recovery is expected to lag spectral indicators of vegetation regrowth (Fernández-Guisuraga et al., 2022; Schellenberg et al., 2023). The slower recovery trajectory observed in R-VSPI highlights its suitability for long-term monitoring of structural regeneration, distinguishing it from optical indices that respond more immediately to early-stage vegetation changes (Chhabra et al., 2022).

5.1.2. Sensitivity of VSPI across pre-fire, immediate post-fire, and one-year post-fire conditions

VSPI consistently exhibits low values (Fig. 5A), indicative of healthy vegetation with strong photosynthetic activity. As an optical index based on SWIR bands, VSPI is influenced by biochemical and physiological vegetation properties, including lignin, cellulose content, and moisture levels (Kokaly and Clark, 1999; Massetti et al., 2019). This confirms that prior to the wildfire, the study region experienced minimal environmental stressors such as drought, disease, or degradation, further reinforcing the baseline conditions captured by R-VSPI. The VSPI map (Fig. 5B) showed a distinct increase in VSPI values, that highlights extensive vegetation stress across the south-eastern coastline, indicating that the wildfire-induced changes predominantly reflected leaf-level biochemical and physiological properties but also indirectly reflected structural loss, particularly in the SWIR bands, where vegetation water content, lignin, cellulose, and canopy biomass strongly influence reflectance and, therefore, VSPI (Elvidge, 1990; Kokaly et al., 2009; Massetti et al., 2019). A notable observation is that in some regions, VSPI increased (Fig. 5B) while R-VSPI remained neutral (Fig. 4B). This pattern suggests wildfire primarily affected canopy foliage and fine branches (<2.5 cm diameter), while larger structural components such as stems and trunks remained intact (Bennett et al., 2016). This discrepancy is particularly relevant in mixed vegetation zones, where understory loss or moderate leaf scorching may cause a strong spectral response without significantly altering SAR backscatter (Tanase et al., 2011; Jimeno-Llorente et al., 2023). The VSPI values decline significantly (Fig. 5C) compared to the immediate post-fire period (Fig. 5B), reflect widespread spectral recovery, but at different rates and in different regions. Areas that previously showed strong spectral disturbance now exhibit lower VSPI values, particularly in northern and inland regions where early vegetation regrowth is more prominent (Fig. 5C) as these areas experienced less severe wildfires in early months of the 2019/20 wildfire season (Filkov et al., 2020; Hislop et al., 2023). This suggests that VSPI is more responsive to the surface and near-surface vegetation, such as shrubs and grasses, which regrow quickly. While this spectral recovery may be interpreted as post-fire forest regrowth, it primarily reflects early successional vegetation rather than complete canopy restoration (Massetti et al., 2019).

5.2. Validating R-VSPI and VSPI sensitivities using field-surveyed data

5.2.1. Immediate post-fire sensitivity of R-VSPI and VSPI

The violin plots (Fig. 6) highlight the distinct and complementary sensitivities of SAR-based R-VSPI and optical-based VSPI to wildfire-induced vegetation damage across defined fire severity classes. The results indicate that R-VSPI and VSPI respond differently due to their inherent sensitivities to different components of vegetation structure and physiology. The R-VSPI values (Fig. 6A) reveal clear trends in SAR sensitivity to wildfire-induced structural vegetation damage, with increasing fire severity associated with more negative R-VSPI values, indicative of greater woody biomass degradation, such as stems and branches, rather than subtle foliage changes (Westman and Paris, 1987; Tanase et al., 2015a, 2015b). Immediately post-fire, 'Low' severity (primarily surface-level, leaving canopy largely intact) exhibit R-VSPI values similar to those in unburnt areas, reflecting minimal structural impacts. However, the R-VSPI distributions show notable overlaps between 'Moderate', 'High', and 'Extreme' severity classes, highlighting a

limitation in distinguishing intermediate canopy scorching from severe canopy biomass loss. This occurs because Sentinel-1 C-band SAR primarily captures structural components, rather than subtle changes in foliage or partial canopy scorch (Fernandez-Carrillo et al., 2019; Chhabra et al., 2022). Consequently, even severely scorched canopies with significant foliage loss may remain structurally similar to less damaged areas if woody biomass structures remain standing, causing SAR-based R-VSPI to underestimate canopy-level disturbances (Tanase et al., 2010; Le Toan et al., 2011). Although this structural sensitivity allows R-VSPI to effectively differentiate 'Moderate' from 'Unburnt' or 'Low' severity classes, it poses challenges in accurately quantifying the most severe canopy-level disturbances, since standing dead biomass continues contributing significantly to backscatter signals post-fire (Flores-Anderson et al., 2019).

In contrast, VSPI (Fig. 6B) effectively captures immediate physiological impacts of wildfire at the canopy level, displaying a clear progression towards higher values with increasing fire severity. This distinct sensitivity primarily results from its reliance on optical short-wave infrared (SWIR) reflectance, which responds directly to canopy moisture loss, foliage greenness, and photosynthetic activity (Kokaly and Clark, 1999; Massetti et al., 2019). Immediately post-fire, VSPI clearly differentiates 'Moderate', 'High', and 'Extreme' severity classes, accurately reflecting the fire severity definitions (>90% canopy scorch or biomass loss) due to extensive foliage destruction significantly altering SWIR spectral signatures. Unlike SAR-based indices, VSPI does not retain influence from residual woody structures, thus effectively identifying severe canopy foliage loss.

5.2.2. One-year post-fire sensitivity of R-VSPI and VSPI

One-year post-fire, R-VSPI maintains its focus on structural integrity (Fig. 6A). Its values continue to reflect long-term biomass loss and the slower recovery rates of larger woody structures. Since R-VSPI is less influenced by rapid regrowth of foliage or understory, it provides a consistent measure of structural recovery over time (Tanase et al., 2011). This long-term sensitivity makes R-VSPI a valuable tool for tracking prolonged recovery trajectories in post-fire environments (Chhabra et al., 2022). Whereas VSPI values in Fig. 6B exhibit increased variability and notable overlap among 'Moderate', 'High', and 'Extreme' severity classes, reflecting partial canopy recovery or understory regrowth. Such regrowth can reintroduce moisture and photosynthetic activity, complicating optical spectral signatures and causing ambiguity in severity interpretations at later stages (Massetti et al., 2019; Gibson et al., 2022). Therefore, while VSPI excels at immediate post-fire canopy damage detection, its long-term effectiveness diminishes as recovering vegetation obscures clear severity delineations, underscoring the temporal limitations of relying solely on optical metrics (Hu et al., 2023) for sustained post-fire severity assessments.

5.3. Implications of fire severity models and classification performance

This study introduces DBHL as a novel fire severity classification model that integrates multi-sensor satellite measurements from passive optical (Sentinel-2) and active SAR (Sentinel-1) sensors. DBHL provides a quantitative assessment of the 2019/20 wildfire impact on south-eastern Australian forests, leveraging the complementary strengths of SAR's structural sensitivity (Le Toan et al., 1992; Tanase et al., 2010) and optical indices' biochemical and spectral insights (Massetti et al., 2019). By integrating structural and spectral fire severity indicators, DBHL advances wildfire impact research and addresses the need for a scalable, interpretable, and operationally viable fire severity model overcoming limitations of previous studies (Collins et al., 2020; Collins et al., 2019; Gibson et al., 2020; Dixon et al., 2022). Unlike deep learning models that require extensive retraining with large historical fire datasets (Zhang et al., 2021; Belenguer-Plomer et al., 2021; Hu et al., 2023), DBHL is computationally efficient, and well-suited for near-real-time disaster response. This near-real-time applicability is enabled as it

leverages SAR's all-weather, day-and-night imaging capabilities (García et al., 2024) and enhances acquisition frequency (Chastain et al., 2019), providing consistent and timely fire severity assessments essential for effective post-fire monitoring and recovery planning (Parks et al., 2014). These assessments are driven by the advanced SAR- and optical-based change detection indices, R-VSPI and VSPI, which have demonstrated higher consistency and reliability compared to conventional indices (Masseti et al., 2019; Chhabra et al., 2022).

All three classification approaches R-VSPI, VSPI, and DBHL used the fire severity scheme that aligns with the existing fire severity standards in Victoria (Collins et al., 2020) and New South Wales (Gibson et al., 2020) (Table 1). Fig. 8A showed that the R-VSPI struggled with differentiating canopy-level severities, as reflected by lower accuracy (OA=66.67%, Kappa=0.58). This limitation stems from the characteristics of C-band SAR backscatter, which has a longer wavelength (5 cm) and penetrates deeper into vegetation layers, making it highly responsive to structural changes in woody vegetation but less sensitive to fine-scale canopy foliage reduction (Tanase et al., 2010; Fernandez-Carrillo et al., 2019). While this sensitivity allows R-VSPI to accurately classify 'Unburnt' (PA=100%, UA=100%) and 'Low' severity (PA=100%, UA=100%), it fails to distinguish higher-severity classes where canopy foliage is consumed but the structural integrity of the stand remains. Consequently, in regions where wildfire led to extensive canopy scorching without complete structural collapse, R-VSPI underestimated severity, misclassifying areas with severe canopy damage as 'Moderate' (PA=66%, UA=33%) or 'High' (PA=60%, UA=75%) rather than 'Extreme' (0% PA and UA). This misclassification pattern aligns with Table 1's fire severity definitions, which indicate that 'Extreme' severity corresponds to $\geq 50\%$ canopy biomass loss. Furthermore, Fig. 6A reinforces the R-VSPI-based fire severity classification model's inability to separate higher severity classes effectively.

In contrast, VSPI as a severity classifier achieved a moderate performance (OA=72.22%, Kappa=0.66), showing improved differentiation of 'Extreme' (PA=100%, UA=100%) severity compared to R-VSPI. This superior performance stems from VSPI's reliance on SWIR reflectance, which is highly sensitive to vegetation water content and canopy foliage loss (Masseti et al., 2019), key indicators of severe canopy scorching or consumption. However, VSPI also tends to overestimate fire severity, particularly in areas where the canopy is scorched but the underlying vegetation structure remains intact. As shown in Fig. 8B, post-fire class separation highlights distinct severity groupings but also misclassifies 'Moderate' (PA=100%, UA=50%) severity as 'High' severity due to SWIR reflectance declining sharply with foliar moisture loss and leaf area reduction, even when woody biomass remains largely unaffected. Additionally, VSPI struggles to distinguish 'Unburnt' (PA=50%, UA=100%) from 'Low' (PA=100%, UA=60%) severity due to residual understory moisture and early-stage regrowth, reflecting spectral confusion between lightly burned areas and regions with residual understory moisture and early-stage regrowth. This limitation is most evident in regions where surface burns minimally affect canopy greenness but still lead to misclassification due to subtle SWIR spectral shifts.

The DBHL model demonstrated superior fire severity classification, achieving the highest overall accuracy (OA = 88.89%, Kappa=0.86) compared to standalone R-VSPI and VSPI classifications in this study. Its performance aligns with high-performing fire severity models in previous studies, such as Dixon et al. (2022) reported an OA of 88.5% across multiple wildfires, and Collins et al. (2020) achieved a similar OA of 88% for south-eastern Australian forests. DBHL resolves these single sensor limitations observed in this study by applying decision-based rules that adaptively combine the strengths of SAR's structural insights with optical spectral sensitivity. This effectively leverages R-VSPI's ability to detect woody biomass degradation and VSPI's capacity to capture canopy loss. This results in significant improvements across all severity classes, particularly for 'Moderate' (PA=100%, UA=75%), 'High' (PA=80%, UA=100%), and 'Extreme' (PA=66.67%,

UA=66.67%) severity classes (Fig. 8C). DBHL outperforms previous studies that reported challenges in detecting burned understory beneath an intact canopy. Dixon et al. (2022) found that 'Low' severity was frequently misclassified (PA=76.4%, UA=80.2%) due to the limitations of optical indices in capturing understory wildfire impacts. Similarly, Collins et al. (2020) reported even lower PA/UA values (~72.9% and 79.7%) for 'Low' severity.

Unlike VSPI, DBHL correctly categorizes areas where structural damage is evident but partial canopy remains, effectively differentiating between 'Moderate' and 'High' severity classes (Tanase et al., 2011). Fig. 8C further illustrates DBHL's advantage in class separation, showing greater distinction between severity levels compared to the individual indices, confirming that the model reduces ambiguity and better reflects vertical vegetation strata impacts. The integration also mitigates confusion between 'Unburnt' and 'Low' severity classes, as DBHL correctly identifies 'Unburnt' areas with 100% PA and UA, compared to 50% PA in VSPI.

Another significant advancement of DBHL is its ability to explicitly label 'Contrasting' regions where R-VSPI and VSPI classifications diverged in complex severity patterns (Fig. 7C, blue colored areas). The 'Contrasting' class pixels coincided with zones affected by severe pre-fire drought, as identified by Nguyen et al. (2021), which triggered substantial foliage loss, a phenomenon described as 'canopy collapse' before the wildfire event (Nolan et al., 2021). The difference between R-VSPI and VSPI in this case is due to drought impacting vegetation plant physiology, leading to decreased photosynthesis and leaf water content (Konings et al., 2021). These changes are detected by VSPI, which uses data from shortwave infrared bands sensitive to leaf moisture and overall plant health (Masseti et al., 2019). In contrast, R-VSPI, based on SAR backscatter, represents forest structure and biomass dynamics more so than physiological states of the vegetation (Le Toan et al., 1992). These discrepancies highlight the complementary nature of SAR and optical indices, particularly in landscapes where canopy wildfire effects and sub-canopy burning produce mixed fire severity signals (Lehmann et al., 2015; Fernandez-Carrillo et al., 2019).

5.4. Limitations and future research directions

A key advancement of this research is the integration of multi-sensor remote sensing data, combining complementary sensitivities of SAR (structural) and optical (physiological) datasets to effectively quantify the eucalyptus forest conditions across pre-fire, immediate post-fire, and one-year post-fire periods. However, some limitations exist. Although the field data represented multiple wildfires and a range of fire severities, the number of validation points was still distinctively limited. Their strategic spatial distribution helped reduce uncertainty but also restricted statistical generalization (Wulder et al., 2019). The confusion matrices in Fig. 8 are therefore presented as an initial demonstration of the DBHL model's potential under a constrained and limited validation, rather than a definitive evaluation and generalization. Within the DBHL framework itself, reliance on a single index in the absence of the other can introduce sensor-specific bias, and severity estimates are sensitive to the percentile-based thresholds used for class definition. While thresholds were derived from a statistically representative sample and validated against independent field and satellite imagery, they may require recalibration when applied to other ecosystems, fire regimes, or sensor configurations. Future work will expand the validation dataset, explore adaptive thresholding approaches, and test the DBHL framework across bioregions and forest types.

Additionally, soil moisture variations can influence SAR backscatter and consequently affect severity mapping accuracy (Ruecker and Siebert, 2000; Gimeno and San-Miguel-Ayanz, 2004; Imperatore et al., 2017), but these effects were not explicitly accounted for or removed in the current study, introducing potential uncertainties in SAR-derived severity assessments. Moreover, the DBHL model is currently calibrated specifically for eucalyptus forests in south-eastern Australia; thus,

its broader applicability to structurally different ecosystems, such as tropical or boreal forests, requires further testing and validation (Pettorelli et al., 2018).

As soil moisture variations influence C-band SAR backscatter, affecting the importance of VV and VH polarizations (Van Zyl et al., 2011; Belenguer-Plomer et al., 2019), future studies should incorporate accurate, high-resolution soil moisture products. Current global datasets (e.g., SMAP at 9 km or CCI at 0.25° resolution) remain insufficiently detailed; thus, forthcoming research should leverage emerging higher-resolution soil moisture datasets to dynamically adjust the weighting of VV and VH polarizations in severity classification (Belenguer-Plomer et al., 2019). SAR-based fire severity assessments also depend significantly on wavelength selection. C-band SAR (Sentinel-1) demonstrates structural sensitivity but limited canopy penetration, potentially restricting differentiation of deeper structural changes (Tanase et al., 2015a, 2015b; Chuvieco et al., 2020). To address this, future studies should integrate additional SAR wavelengths, particularly longer wavelengths such as L-band (1.25 GHz) NASA/ISRO Synthetic Aperture RADAR (NISAR; Rosen et al., 2015), and P-band (0.43 GHz) from ESA's BIOMASS (Le Toan et al., 2011). These longer wavelengths provide greater penetration through dense vegetation, enhancing discrimination of wildfire-induced structural alterations (Tanase et al., 2015a, 2015b). Additionally, incorporating high-resolution structural datasets like airborne LiDAR would improve characterization of understory and fine-scale structural complexity, complementing spaceborne observations (Hu et al., 2019; García et al., 2020; Woodgate et al., 2025).

6. Conclusion

This study demonstrates the effectiveness of DBHL as a multi-sensor fire severity classification model, integrating optical and SAR data. A pixel-wise linear regression was applied to spatially upscale the application of R-VSPI and VSPI for fire severity assessments across wildfire-impacted forests of south-eastern Australia during the 2019/20 Black Summer wildfire season. The R-VSPI and VSPI were computed using Sentinel-1 (VV and VH) and Sentinel-2 (SWIR1 and SWIR2) band pairs, respectively. The results highlight the complementary nature of R-VSPI and VSPI, where R-VSPI is more sensitive to structural changes in woody vegetation, while VSPI effectively captures canopy damage. DBHL outperformed single-sensor approaches, achieving the highest classification accuracy (OA=88.89%, Kappa=0.86), particularly improving differentiation of Moderate (PA=100%, UA=75%) and High-severity (PA=80%, UA=100%) classes. The integration of SAR and optical indices within DBHL enhances fire severity assessments by resolving ambiguities between canopy-level and structural damage. The implementation of DBHL for operational use may enhance near-real-time fire severity monitoring at large-scale, supporting data-driven decisions for emergency response and ecosystem restoration.

CRedit authorship contribution statement

Aakash Chhabra: Writing – review & editing, Writing – original draft, Visualization, Validation, Software, Methodology, Investigation, Formal analysis, Data curation, Conceptualization. **Christoph Rüdiger:** Writing – review & editing, Visualization, Supervision, Resources, Methodology, Conceptualization. **James Hilton:** Writing – review & editing, Visualization, Supervision. **Rachael H. Nolan:** Writing – review & editing, Validation, Resources. **Eli R. Bendall:** Writing – review & editing, Validation, Resources. **Marta Yebra:** Writing – review & editing, Visualization, Validation, Supervision. **Thomas Jagdhuber:** Writing – review & editing, Visualization, Validation, Supervision.

Declaration of competing interest

The authors declare that they have no known competing financial interests or personal relationships that could have appeared to influence

the work reported in this paper.

Data availability

Data will be made available on request.

References

- Allouche, O., Tsoar, A., Kadmon, R., 2006. Assessing the accuracy of species distribution models: prevalence, kappa and the true skill statistic (TSS). *J. Appl. Ecol.* 43 (6), 1223–1232.
- Australian Bureau of Meteorology (BoM). Climate Data Online: Daily rainfall observations. Available at: <https://www.bom.gov.au/climate/data/> (Last Accessed: 11 August 2024).
- Ban, Y., Zhang, P., Nascetti, A., Bevington, A.R., Wulder, M.A., 2020. Near real-time wildfire progression monitoring with Sentinel-1 SAR time series and deep learning. *Sci. Rep.* 10 (1), 1322.
- Baret, F., Buis, S., 2008. Estimating canopy characteristics from remote sensing observations: Review of methods and associated problems. *Adv. Land Remote Sens.: Syst., Model., Invers. Appl.* 173–201.
- Belenguer-Plomer, M.A., Chuvieco, E., Tanase, M.A., 2019. Evaluation of backscatter coefficient temporal indices for burned area mapping. In: *Active and Passive Microwave Remote Sensing for Environmental Monitoring III*, 11154. SPIE, pp. 12–20. October.
- Belenguer-Plomer, M.A., Tanase, M.A., Chuvieco, E., Bovolo, F., 2021. CNN-based burned area mapping using radar and optical data. *Remote Sens. Environ.* 260, 112468.
- Bennett, L.T., Bruce, M.J., MacHunter, J., Kohout, M., Tanase, M.A., Aponte, C., 2016. Mortality and recruitment of fire-tolerant eucalypts as influenced by wildfire severity and recent prescribed fire. *For. Ecol. Manag.* 380, 107–117.
- Boer, M.M., Resco de Dios, V., Bradstock, R.A., 2020. Unprecedented burn area of Australian mega forest fires. *Nat. Clim. Chang.* 10 (3), 171–172.
- Bourgeau-Chavez, L.L., Harrell, P.A., Kasischke, E.S., French, N.H.F., 1997. The detection and mapping of Alaskan wildfires using a spaceborne imaging radar system. *Int. J. Remote Sens.* 18 (2), 355–373.
- Bourgeau-Chavez, L.L., Kasischke, E.S., Riordan, K., Brunzell, S., Nolan, M., Hyer, E., Slawski, J., Medvecz, M., Walters, T., Ames, S., 2007. Remote monitoring of spatial and temporal surface soil moisture in fire disturbed boreal forest ecosystems with ERS SAR imagery. *Int. J. Remote Sens.* 28 (10), 2133–2162.
- Bowman, D.M., Kolden, C.A., Abatzoglou, J.T., Johnston, F.H., van der Werf, G.R., Flannigan, M., 2020. Vegetation fires in the Anthropocene. *Nat. Rev. Earth & Environ.* 1 (10), 500–515.
- Bowman, D.M., Williamson, G.J., Gibson, R.K., Bradstock, R.A., Keenan, R.J., 2021. The severity and extent of the Australia 2019–20 Eucalyptus Forest fires are not the legacy of forest management. *Nat. Ecol. Evol.* 5 (7), 1003–1010.
- Bradstock, R.A., Hammill, K.A., Collins, L., Price, O., 2010. Effects of weather, fuel and terrain on fire severity in topographically diverse landscapes of south-eastern Australia. *Landsc. Ecol.* 25, 607–619.
- Cardil, A., Mola-Yudego, B., Blázquez-Casado, Á., González-Olabarria, J.R., 2019. Fire and burn severity assessment: Calibration of Relative Differenced Normalized Burn Ratio (RdNBR) with field data. *J. Environ. Manag.* 235, 342–349.
- Chastain, R., Housman, I., Goldstein, J., Finco, M., Tenneson, K., 2019. Empirical cross sensor comparison of Sentinel-2A and 2B MSI, Landsat-8 OLI, and Landsat-7 ETM+ top of atmosphere spectral characteristics over the conterminous United States. *Remote Sens. Environ.* 221, 274–285.
- Chhabra, A., Rüdiger, C., Yebra, M., Jagdhuber, T., Hilton, J., 2022. RADAR-vegetation structural perpendicular index (R-VSP) for the quantification of wildfire impact and post-fire vegetation recovery. *Remote Sens.* 14 (13), 3132.
- Chuvieco, E., Riaño, D., Danson, F.M., Martin, P., 2006. Use of a radiative transfer model to simulate the postfire spectral response to burn severity. *J. Geophys. Res. Biogeosci.* 111 (G4).
- Chuvieco, E., Aguado, I., Salas, J., García, M., Yebra, M., Oliva, P., 2020. Satellite remote sensing contributions to wildland fire science and management. *Curr. For. Rep.* 6, 81–96.
- Cloude, S.R., Pottier, E., 2002. A review of target decomposition theorems in radar polarimetry. *IEEE Trans. Geosci. Remote Sens.* 34 (2), 498–518.
- Collins, L., Bradstock, R.A., Penman, T.D., 2014. Can precipitation influence landscape controls on wildfire severity? A case study within temperate eucalypt forests of south-eastern Australia. *Int. J. Wildland Fire* 23 (1), 9–20.
- Collins, L., Bennett, A.F., Leonard, S.W., Penman, T.D., 2019. Wildfire refugia in forests: Severe fire weather and drought mute the influence of topography and fuel age. *Glob. Chang. Biol.* 25 (11), 3829–3843.
- Collins, L., McCarthy, G., Mellor, A., Newell, G., Smith, L., 2020. Training data requirements for fire severity mapping using Landsat imagery and random forest. *Remote Sens. Environ.* 245, 111839.
- Collins, L., Bradstock, R.A., Clarke, H., Clarke, M.F., Nolan, R.H., Penman, T.D., 2021. The 2019/2020 mega-fires exposed Australian ecosystems to an unprecedented extent of high-severity fire. *Environ. Res. Lett.* 16 (4), 044029.
- Congalton, R.G., Green, K., 2019. *Assessing the accuracy of remotely sensed data: principles and practices*. CRC press.
- Crowley, M.A., Cardille, J.A., White, J.C., Wulder, M.A., 2019. Generating intra-year metrics of wildfire progression using multiple open-access satellite data streams. *Remote Sens. Environ.* 232, 111295.

- Curran, P.J., 1989. Remote sensing of foliar chemistry. *Remote Sens. Environ.* 30 (3), 271–278.
- Davey, S.M., Sarre, A., 2020. The 2019/20 Black Summer bushfires. *Aust. For.* 83 (2), 47–51.
- Dixon, D.J., Callow, J.N., Duncan, J.M., Setterfield, S.A., Pauli, N., 2022. Regional-scale fire severity mapping of Eucalyptus forests with the Landsat archive. *Remote Sens. Environ.* 270, 112863.
- Driscoll, D.A., Macdonald, K.J., Gibson, R.K., Doherty, T.S., Nimmo, D.G., Nolan, R.H., Ritchie, E.G., Williamson, G.J., Heard, G.W., Tasker, E.M., Bilney, R., 2024. Biodiversity impacts of the 2019–2020 Australian megafires. *Nature* 1–8.
- Drusch, M., Del Bello, U., Carlier, S., Colin, O., Fernandez, V., Gascon, F., Hoersch, B., Isola, C., Laberinti, P., Martimort, P., Meygret, A., 2012. Sentinel-2: ESA's optical high-resolution mission for GMES operational services. *Remote Sens. Environ.* 120, 25–36.
- Elvidge, C.D., 1990. Visible and near infrared reflectance characteristics of dry plant materials. *Remote Sens.* 11 (10), 1775–1795.
- Engelbrecht, J., Theron, A., Vhengani, L., Kemp, J., 2017. A simple normalized difference approach to burnt area mapping using multi-polarisation C-Band SAR. *Remote Sens.* 9 (8), 764.
- Escuin, S., Navarro, R., Fernández, P., 2008. Fire severity assessment by using NBR (Normalized Burn Ratio) and NDVI (Normalized Difference Vegetation Index) derived from LANDSAT TM/ETM images. *Int. J. Remote Sens.* 29 (4), 1053–1073.
- Fernandez-Carrillo, A., McCaw, L., Tanase, M.A., 2019. Estimating prescribed fire impacts and post-fire tree survival in eucalyptus forests of Western Australia with L-band SAR data. *Remote Sens. Environ.* 224, 133–144.
- Fernández-Guisuraga, J.M., Marcos, E., Suárez-Seoane, S., Calvo, L., 2022. ALOS-2 L-band SAR backscatter data improves the estimation and temporal transferability of wildfire effects on soil properties under different post-fire vegetation responses. *Sci. Total Environ.* 842, 156852.
- Filkov, A.I., Ngo, T., Matthews, S., Telfer, S., Penman, T.D., 2020. Impact of Australia's catastrophic 2019/20 bushfire season on communities and environment. Retrospective analysis and current trends. *J. Safety Sci. Resil.* 1 (1), 44–56.
- Flores-Anderson, A.I., Herndon, K.E., Thapa, R.B., Cherrington, E., 2019. The SAR handbook: Comprehensive methodologies for forest monitoring and biomass estimation, No. MSFC-E-DAA-TN67454.
- Frantz, D., Schug, F., Okujeni, A., Navacchi, C., Wagner, W., van der Linden, S., Hostert, P., 2021. National-scale mapping of building height using Sentinel-1 and Sentinel-2 time series. *Remote Sens. Environ.* 252, 112128.
- García, L.P., Furano, G., Ghiglione, M., Zancan, V., Imbembo, E., Ilioudis, C., Clemente, C., Trucco, P., 2024. Advancements in onboard processing of synthetic aperture radar (sar) data: Enhancing efficiency and real-time capabilities. *IEEE Journal of Selected Topics in Applied Earth Observations and Remote Sensing* 17, 16625–16645.
- García, M., North, P., Viana-Soto, A., Stavros, N.E., Rosette, J., Martín, M.P., Franquesa, M., González-Cascón, R., Riaño, D., Becerra, J., Zhao, K., 2020. Evaluating the potential of LiDAR data for fire damage assessment: A radiative transfer model approach. *Remote Sens. Environ.* 247, 111893.
- Gibson, R., Danaher, T., Hehir, W., Collins, L., 2020. A remote sensing approach to mapping fire severity in south-eastern Australia using sentinel 2 and random forest. *Remote Sens. Environ.* 240, 111702.
- Gibson, R.K., White, L.A., Hislop, S., Nolan, R.H., Dorrrough, J., 2022. The post-fire stability index; a new approach to monitoring post-fire recovery by satellite imagery. *Remote Sens. Environ.* 280, 113151.
- Giglio, L., Boschetti, L., Roy, D.P., Humber, M.L., Justice, C.O., 2018. The Collection 6 MODIS burned area mapping algorithm and product. *Remote Sens. Environ.* 217, 72–85.
- Gimeno, M., San-Miguel-Ayanz, J., 2004. Evaluation of RADARSAT-1 data for identification of burnt areas in Southern Europe. *Remote Sens. Environ.* 92 (3), 370–375.
- Gorelick, N., Hancher, M., Dixon, M., Ilyushchenko, S., Thau, D., Moore, R., 2017. Google Earth Engine: Planetary-scale geospatial analysis for everyone. *Remote Sens. Environ.* 202, 18–27.
- Harris, L., Taylor, A.H., 2015. Topography, fuels, and fire exclusion drive fire severity of the Rim Fire in an old-growth mixed-conifer forest, Yosemite National Park, USA. *Ecosystems* 18, 1192–1208.
- Hislop, S., Stone, C., Gibson, R.K., Roff, A., Choat, B., Nolan, R.H., Nguyen, T.H., Carnegie, A.J., 2023. Using dense Sentinel-2 time series to explore combined fire and drought impacts in eucalypt forests. *Frontiers in Forests and Global Change* 6, 1018936.
- Hu, T., Ma, Q., Su, Y., Battles, J.J., Collins, B.M., Stephens, S.L., Kelly, M., Guo, Q., 2019. A simple and integrated approach for fire severity assessment using bi-temporal airborne LiDAR data. *Int. J. Appl. Earth Obs. Geoinf.* 78, 25–38.
- Hu, X., Zhang, P., Ban, Y., Rahnemoonfar, M., 2023. GAN-based SAR and optical image translation for wildfire impact assessment using multi-source remote sensing data. *Remote Sens. Environ.* 289, 113522.
- Hutchinson, M.F., McIntyre, S., Hobbs, R.J., Stein, J.L., Garnett, S., Kinloch, J., 2005. Integrating a global agro-climatic classification with bioregional boundaries in Australia. *Glob. Ecol. Biogeogr.* 14 (3), 197–212.
- IBRA (2017). Interim biogeographic regionalisation for Australia (IBRA). Available online at: <https://www.dceew.gov.au/environment/land/nrs/science/ibra> (accessed June 23, 2024).
- Imperatore, P., Azar, R., Calo, F., Stroppiana, D., Brivio, P.A., Lanari, R., Pepe, A., 2017. Effect of the vegetation fire on backscattering: An investigation based on Sentinel-1 observations. *IEEE Journal of Selected Topics in Applied Earth Observations and Remote Sensing* 10 (10), 4478–4492.
- Jacquemoud, S., Verhoef, W., Baret, F., Bacour, C., Zarco-Tejada, P.J., Asner, G.P., François, C., Ustin, S.L., 2009. PROSPECT+ SAIL models: A review of use for vegetation characterization. *Remote Sens. Environ.* 113, S56–S66.
- Jimeno-Llorente, L., Marcos, E., Fernández-Guisuraga, J.M., 2023. The Effects of Fire Severity on Vegetation Structural Complexity Assessed Using SAR Data Are Modulated by Plant Community Types in Mediterranean Fire-Prone Ecosystems. *Fire* 6 (12), 450.
- Keeley, J.E., 2009. Fire intensity, fire severity and burn severity: a brief review and suggested usage. *Int. J. Wildland Fire* 18 (1), 116–126.
- Keith, D.A., 2004. Ocean shores to desert dunes: the native vegetation of NSW and the ACT Department of Environment and Conservation. NSW.
- Kim, Y., Jackson, T., Bindlish, R., Lee, H., Hong, S., 2011. Radar vegetation index for estimating the vegetation water content of rice and soybean. *IEEE Geosci. Remote Sens. Lett.* 9 (4), 564–568.
- Kokaly, R.F., Clark, R.N., 1999. Spectroscopic determination of leaf biochemistry using band-depth analysis of absorption features and stepwise multiple linear regression. *Remote Sens. Environ.* 67 (3), 267–287.
- Kokaly, R.F., Asner, G.P., Ollinger, S.V., Martin, M.E., Wessman, C.A., 2009. Characterizing canopy biochemistry from imaging spectroscopy and its application to ecosystem studies. *Remote Sens. Environ.* 113, S78–S91.
- Konings, A.G., Saatchi, S.S., Frankenberg, C., Keller, M., Leshyk, V., Anderegg, W.R., Humphrey, V., Matheny, A.M., Trugman, A., Sack, L., Agee, E., 2021. Detecting forest response to droughts with global observations of vegetation water content. *Glob. Chang. Biol.* 27 (23), 6005–6024.
- Le Breton, T.D., Lyons, M.B., Nolan, R.H., Penman, T., Williamson, G.J., Ooi, M.K., 2022. Megafire-induced interval squeeze threatens vegetation at landscape scales. *Front. Ecol. Environ.* 20 (5), 327–334.
- Le Toan, T., Beaudoin, A., Riom, J., Guyon, D., 1992. Relating forest biomass to SAR data. *IEEE Trans. Geosci. Remote Sens.* 30 (2), 403–411.
- Le Toan, T., Quegan, S., Davidson, M.W.J., Balzer, H., Paillou, P., Papathanassiou, K., Plummer, S., Rocca, F., Saatchi, S., Shugart, H., Ulander, L., 2011. The BIOMASS mission: Mapping global forest biomass to better understand the terrestrial carbon cycle. *Remote Sens. Environ.* 115 (11), 2850–2860.
- Lehmann, E.A., Caccetta, P., Lowell, K., Mitchell, A., Zhou, Z.S., Held, A., Milne, T., Tapley, I., 2015. SAR and optical remote sensing: Assessment of complementarity and interoperability in the context of a large-scale operational forest monitoring system. *Remote Sens. Environ.* 156, 335–348.
- Lentile, L.B., Holden, Z.A., Smith, A.M., Falkowski, M.J., Hudak, A.T., Morgan, P., Lewis, S.A., Gessler, P.E., Benson, N.C., 2006. Remote sensing techniques to assess active fire characteristics and post-fire effects. *Int. J. Wildland Fire* 15 (3), 319–345.
- Lindenmayer, D.B., Taylor, C., 2020. New spatial analyses of Australian wildfires highlight the need for new fire, resource, and conservation policies. *Proc. Natl. Acad. Sci.* 117 (22), 12481–12485.
- Littell, J.S., McKenzie, D., Wan, H.Y., Cushman, S.A., 2018. Climate change and future wildfire in the western United States: An ecological approach to nonstationarity. *Earth's Future* 6 (8), 1097–1111.
- Lozano, O.M., Salis, M., Ager, A.A., Arca, B., Alcasena, F.J., Monteiro, A.T., Finney, M.A., Del Giudice, L., Scoccimarro, E., Spano, D., 2017. Assessing climate change impacts on wildfire exposure in Mediterranean areas. *Risk Anal.* 37 (10), 1898–1916.
- Massetti, A., Rüdiger, C., Yebra, M., Hilton, J., 2019. The Vegetation Structure Perpendicular Index (VSPDI): A forest condition index for wildfire predictions. *Remote Sens. Environ.* 224, 167–181.
- Miller, R.G., Tangney, R., Enright, N.J., Fontaine, J.B., Merritt, D.J., Ooi, M.K., Ruthrof, K.X., Miller, B.P., 2019. Mechanisms of fire seasonality effects on plant populations. *Trends Ecol. Evol.* 34 (12), 1104–1117.
- Mitchard, E.T., Saatchi, S.S., White, L.J., Abernethy, K.A., Jeffery, K.J., Lewis, S.L., Collins, M., Lefsky, M.A., Leal, M.E., Woodhouse, I.H., Meir, P., 2012. Mapping tropical forest biomass with radar and spaceborne LiDAR in Lopé National Park, Gabon: overcoming problems of high biomass and persistent cloud. *Biogeosciences* 9 (1), 179–191.
- Montreal Process Implementation Group for Australia and National Forest Inventory Steering Committee, 2018. Australia's state of the forests report 2018. Montreal Process Implementation Group for Australia and National Forest Inventory Steering Committee, Canberra.
- Morgan, P., Keane, R.E., Dillon, G.K., Jain, T.B., Hudak, A.T., Karau, E.C., Sikkink, P.G., Holden, Z.A., Strand, E.K., 2014. Challenges of assessing fire and burn severity using field measures, remote sensing and modelling. *Int. J. Wildland Fire* 23 (8), 1045–1060.
- Navarro-Sanchez, V.D., Lopez-Sanchez, J.M., Ferro-Famil, L., 2013. Polarimetric approaches for persistent scatterers interferometry. *IEEE Trans. Geosci. Remote Sens.* 52 (3), 1667–1676.
- Nguyen, H., Wheeler, M.C., Hendon, H.H., Lim, E.P., Otkin, J.A., 2021. The 2019 flash droughts in subtropical eastern Australia and their association with large-scale climate drivers. *Wea. Clim. Extrem.* 32, 100321.
- Nolan, R.H., Gauthey, A., Lasso, A., Medlyn, B.E., Smith, R., Chhajer, S.S., Fuller, K., Song, M., Li, X., Beaumont, L.J., Boer, M.M., 2021. Hydraulic failure and tree size linked with canopy die-back in eucalypt forest during extreme drought. *New Phytol.* 230 (4), 1354–1365.
- Nolan, R.H., Collins, L., Gibson, R.K., Samson, S.A., Rolls, K.T., Milner, K., Medlyn, B.E., Price, O.F., Griebel, A., Choat, B., Jiang, M., 2022. The carbon cost of the 2019–20 Australian fires varies with fire severity and forest type. *Glob. Ecol. Biogeogr.* 31 (10), 2131–2146.
- Nolan, R.H., Gibson, R.K., Cirulis, B., Holyland, B., Samson, S.A., Jenkins, M., Penman, T., Boer, M.M., 2024. Incorporating burn heterogeneity with fuel load estimates may improve fire behaviour predictions in south-east Australian eucalypt forest. *Int. J. Wildland Fire* 33 (3).

- Parks, S.A., Dillon, G.K., Miller, C., 2014. A new metric for quantifying burn severity: the relativized burn ratio. *Remote Sens.* 6 (3), 1827–1844.
- Pedregosa, F., Varoquaux, G., Gramfort, A., Michel, V., Thirion, B., Grisel, O., Blondel, M., Prettenhofer, P., Weiss, R., Dubourg, V., Vanderplas, J., 2011. Scikit-learn: Machine learning in Python. *J. Mach. Learn. Res.* 12, 2825–2830.
- Pettorelli, N., Schulte to Bühne, H., Tulloch, A., Dubois, G., Macinnis-Ng, C., Queirós, A. M., Keith, D.A., Wegmann, M., Schrodt, F., Stellmes, M., Sonnenschein, R., 2018. Satellite remote sensing of ecosystem functions: opportunities, challenges and way forward. *Remote Sens. Ecol. Conserv.* 4 (2), 71–93.
- Quintero, N., Viedma, O., Veraverbeke, S., Moreno, J.M., 2025. Optimising fire severity mapping using pixel-based image compositing. *Remote Sens. Environ.* 321, 114687.
- Reiche, J., Verbesselt, J., Hoekman, D., Herold, M., 2015. Fusing Landsat and SAR time series to detect deforestation in the tropics. *Remote Sens. Environ.* 156, 276–293.
- Rouse Jr., J., Haas, R.H., Deering, D., Schell, J., Harlan, J.C., 1974. Monitoring the Vernal Advancement and Retrogradation (Green Wave Effect) of Natural Vegetation; No. NASA-CR-132982. NASA, Washington, DC, USA.
- Roy, D.P., Boschetti, L., Trigg, S.N., 2006. Remote sensing of fire severity: assessing the performance of the normalized burn ratio. *IEEE Geosci. Remote Sens. Lett.* 3 (1), 112–116.
- Ruecker, G., Siegert, F., 2000. Burn scar mapping and fire damage assessment using ERS-2 SAR images in East Kalimantan, Indonesia. *Int. Archiv. Photogramm. Remote Sens.* 33 (B7/3; PART 7), 1286–1293.
- Saatchi, S., 2019. SAR methods for mapping and monitoring forest biomass. In: Flores, A., Herndon, K., Thapa, R., Cherrington, E. (Eds.), *SAR Handbook: Comprehensive Methodologies for Forest Monitoring and Biomass Estimation*. Washington, DC, USA, NASA, pp. 207–246.
- Schellenberg, K., Jagdhuber, T., Zehner, M., Hese, S., Urban, M., Urbazaev, M., Hartmann, H., Schmulilius, C., Dubois, C., 2023. Potential of Sentinel-1 SAR to assess damage in drought-affected temperate deciduous broadleaf forests. *Remote Sens.* 15 (4), 1004.
- Story, M., Congalton, R.G., 1986. Accuracy assessment: a user's perspective. *Photogramm. Eng. Remote Sens.* 52 (3), 397–399.
- Stroppiana, D., Azar, R., Calò, F., Pepe, A., Imperatore, P., Boschetti, M., Silva, J.M., Brivio, P.A., Lanari, R., 2015. Integration of optical and SAR data for burned area mapping in Mediterranean Regions. *Remote Sens.* 7 (2), 1320–1345.
- Szigarski, C., Jagdhuber, T., Baur, M., Thiel, C., Parrens, M., Wigneron, J.P., Piles, M., Entekhabi, D., 2018. Analysis of the radar vegetation index and potential improvements. *Remote Sens.* 10 (11), 1776.
- Tanase, M.A., Santoro, M., Wegmüller, U., de la Riva, J., Pérez-Cabello, F., 2010. Properties of X-, C-and L-band repeat-pass interferometric SAR coherence in Mediterranean pine forests affected by fires. *Remote Sens. Environ.* 114 (10), 2182–2194.
- Tanase, M., de la Riva, J., Santoro, M., Pérez-Cabello, F., Kasischke, E., 2011. Sensitivity of SAR data to post-fire forest regrowth in Mediterranean and boreal forests. *Remote Sens. Environ.* 115 (8), 2075–2085.
- Tanase, M.A., Santoro, M., Aponte, C., de la Riva, J., 2013. Polarimetric properties of burned forest areas at C-and L-band. *IEEE J. Selected Top. Appl. Earth Observ. Remote Sens.* 7 (1), 267–276.
- Tanase, M.A., Kennedy, R., Aponte, C., 2015a. Fire severity estimation from space: A comparison of active and passive sensors and their synergy for different forest types. *Int. J. Wildland Fire* 24 (8), 1062–1075.
- Tanase, M.A., Kennedy, R., Aponte, C., 2015b. Radar Burn Ratio for fire severity estimation at canopy level: An example for temperate forests. *Remote Sens. Environ.* 170, 14–31.
- Tanase, M.A., Aponte, C., Mermoz, S., Bouvet, A., Le Toan, T., Heurich, M., 2018. Detection of windthrows and insect outbreaks by L-band SAR: A case study in the Bavarian Forest National Park. *Remote Sens. Environ.* 209, 700–711.
- Taylor, C., McCarthy, M.A., Lindenmayer, D.B., 2014. Nonlinear effects of stand age on fire severity. *Conserv. Lett.* 7 (4), 355–370.
- Torres, R., Snoeij, P., Geudtner, D., Bibby, D., Davidson, M., Attema, E., Potin, P., Rommen, B., Floury, N., Brown, M., Traver, I.N., 2012. GMES Sentinel-1 mission. *Remote Sens. Environ.* 120, 9–24.
- Turner, M.G., Romme, W.H., Gardner, R.H., 1999. Prefire heterogeneity, fire severity, and early postfire plant reestablishment in subalpine forests of Yellowstone National Park, Wyoming. *Int. J. Wildland Fire* 9 (1), 21–36.
- Ulaby, F.T., Long, D.G., 2014. Blackwell W. et al. *Microwave Radar and Radiometric Remote Sensing*. Univ. Michigan Press, Ann Arbor.
- Van Zyl, J.J., Arii, M., Kim, Y., 2011. Model-based decomposition of polarimetric SAR covariance matrices constrained for nonnegative eigenvalues. *IEEE Trans. Geosci. Remote Sens.* 49 (9), 3452–3459.
- Veraverbeke, S., Lhermitte, S., Verstraeten, W.W., Goossens, R., 2011. Evaluation of pre/post-fire differenced spectral indices for assessing burn severity in a Mediterranean environment with Landsat Thematic Mapper. *Int. J. Remote Sens.* 32 (12), 3521–3537.
- Verbyla, D.L., Kasischke, E.S., Hoy, E.E., 2008. Seasonal and topographic effects on estimating fire severity from Landsat TM/ETM+ data. *Int. J. Wildland Fire* 17 (4), 527–534.
- Verrelst, J., Rivera, J.P., Veroustraete, F., Muñoz-Marí, J., Clevers, J.G., Camps-Valls, G., Moreno, J., 2015. Experimental Sentinel-2 LAI estimation using parametric, non-parametric and physical retrieval methods—A comparison. *ISPRS J. Photogramm. Remote Sens.* 108, 260–272.
- Vilà-Vilardell, L., Keeton, W.S., Thom, D., Gyetlshen, C., Tshering, K., Gratzler, G., 2020. Climate change effects on wildfire hazards in the wildland-urban-interface—Blue pine forests of Bhutan. *For. Ecol. Manag.* 461, 117927.
- Vreugdenhil, M., Wagner, W., Bauer-Marschallinger, B., Pfeil, I., Teubner, I., Rüdiger, C., Strauss, P., 2018. Sensitivity of Sentinel-1 backscatter to vegetation dynamics: An Austrian case study. *Remote Sens.* 10 (9), 1396.
- Westman, W.E., Paris, J.F., 1987. Detecting forest structure and biomass with C-band multipolarization radar: Physical model and field tests. *Remote Sens. Environ.* 22 (2), 249–269.
- Woodgate, W., Phinn, S., Devereux, T., Aryal, R.R., 2025. Bushfire recovery at a long-term tall eucalypt flux site through the lens of a satellite: Combining multi-scale data for structural-functional insight. *Remote Sens. Environ.* 317, 114530.
- Wulder, M.A., Loveland, T.R., Roy, D.P., Crawford, C.J., Masek, J.G., Woodcock, C.E., Allen, R.G., Anderson, M.C., Belward, A.S., Cohen, W.B., Dwyer, J., 2019. Current status of Landsat program, science, and applications. *Remote Sens. Environ.* 225, 127–147.
- Yin, C., He, B., Quan, X., Yebra, M., Lai, G., 2020. Remote sensing of burn severity using coupled radiative transfer model: a case study on Chinese Qinyuan Pine fires. *Remote Sens.* 12 (21), 3590.
- Zhang, W., Brandt, M., Wang, Q., Prishchepov, A.V., Tucker, C.J., Li, Y., Lyu, H., Fensholt, R., 2019. From woody cover to woody canopies: How Sentinel-1 and Sentinel-2 data advance the mapping of woody plants in savannas. *Remote Sens. Environ.* 234, 111465.
- Zhang, P., Ban, Y., Nascetti, A., 2021. Learning U-Net without forgetting for near real-time wildfire monitoring by the fusion of SAR and optical time series. *Remote Sens. Environ.* 261, 112467.